A Review of Current Rough Volatility Methods

Noah Beelders

A dissertation submitted to the Faculty of Commerce, University of Cape Town, in partial fulfilment of the requirements for the degree of Master of Philosophy.

September 10, 2021

MPhil in Mathematical Finance,
University of Cape Town.

University of Cape Town

The copyright of this thesis vests in the author. No quotation from it or information derived from it is to be published without full acknowledgement of the source. The thesis is to be used for private study or non-commercial research purposes only.

Published by the University of Cape Town (UCT) in terms of the non-exclusive license granted to UCT by the author.

University of Cape Town

Declaration

I declare that this dissertation is my own, unaided work. It is being submitted for the Degree of Master of Philosophy in the University of the Cape Town. It has not been submitted before for any degree or examination in any other University.

September 10, 2021

Abstract

Recent literature has provided empirical evidence showing that the behaviour of volatility in financial markets is rough. Given the complicated nature of rough dynamics, a review of these methods is presented with the intention of ensuring tractability for those wishing to implement these techniques. The models of rough dynamics are built upon the fractional Brownian Motion and its associated power-law kernel. One such model is called the Rough Heston, an extension of the Classical Heston model, and is the main model of focus for this dissertation. To implement the Rough Heston, fractional Riccati ordinary differential equations (ODEs) must be solved; and this requires numerical methods. Three such methods in order of increasing complexity are considered. Using the fractional Adam's numerical method, the Rough Heston model can be effected to produce realistic volatility smiles comparable to that of market data. Lastly, a quick and easy approximation of the Rough Heston model, called the Poor Man's Heston, is discussed and implemented.

Acknowledgements

To start, I would like to express my gratitude to each member of the African Institute of Financial Markets and Risk Management (AIFMRM). Despite the difficulties of the COVID-19 pandemic, their incessant efforts ensured I was able to continue my studies seamlessly.

Without the help and guidance of my supervisor Mr Andrew Soane, this research would not have been possible. It was an honour being mentored by him, and learning from him. Additionally, I am incredibly grateful for my other lecturers, Peter Ouwehand, Thomas McWalter and Obeid Mahomed, as they taught me the necessary fundamentals to make my research significantly better.

Lastly, the love and support of my family have been pertinent in ensuring my success. Their continuous encouragement allowed me to remain determined and to confidently pursue my passion for learning.

Contents

List of Figures

List of Tables

Chapter 1

Introduction

Option pricing models incorporating a dynamic volatility structure have become increasingly important, given that the volatility smile/skew phenomenon contradicts the Black-Scholes constant volatility assumption. To capture the higher implied volatility for In-The-Money (ITM) and Out-The-Money (OTM) [1] option prices, techniques such as local volatility modelling from Dupire (1994) and stochastic volatility modelling from Heston (1993) have been utilised. However, despite their improvements, these models are still insufficient.

Recently, Gatheral *et al.* (2018) convincingly showed that the volatility implied from market data was sufficiently irregular to be classified as a rough process. By studying the term structure of at-the-money (TS ATM) implied volatility (IV) skew of the market, it was shown that this roughness was best captured by using fractional Brownian Motion (fBM), a fractional calculus generalisation of Brownian Motion (BM) popularised by Mandelbrot and Van Ness (1968). This simple shift from using BM to fBM has shown significant improvements in capturing smile dynamics, and has stimulated further research on models incorporating fBM. Given the additional complexity imposed by fBM, some research has also been centered around increasing the tractability of these models.

The purpose of this dissertation is hence to review developments in this field, with a focus on finding simplifications of existing methods so that fBM models can be more easily utilised in practice. Before discussing any viable models, it is necessary to define fBM and to discuss its essential features. This is done in Section 2.1 of Chapter 2. In Section 2.2 and 2.3, the empirical studies in Gatheral *et al.* (2018) supporting the presence of fBM dynamics in market volatility are discussed. A viable model constructed by El Euch and Rosenbaum (2019) is then introduced and explored in Chapter 3 and a viable approximation of this model that greatly

[1] An ITM option is one which would receive a profit if it were exercised at the current underlying asset price for the given strike price. An OTM option is one which would not be exercised given its current underlying asset price.

simplifies implementation is discussed. This model is called the Rough Heston, and is in fact a fBM generalisation of the classical Heston Model. In the Methodology, Chapter 4, the models are implemented and their viability is discussed.

Chapter 2

Literature Review

2.1 Fractional Brownian Motion

The aforementioned seminal paper of Mandelbrot and Van Ness (1968) popularised the concept of fBM as a generalisation of the BM process of Bachelier, Wiener and Lévy. Contrary to fBM, the ordinary BM process has tractable properties that make it easy to use. For completeness, we state the definition of Brownian motion from Hunt and Kennedy (2004):

Definition 2.1. (Brownian Motion) A Brownian Motion, B_t, is the unique real-valued stochastic process with the following properties:

1. Given any $t_0 < t_1 < ... < t_n$ the random variables $\{(B_{t_i} - B_{t_{i-1}}),\ i = 1, 2, ..., n\}$ are independent
2. For any $0 \leq s \leq t$, $B_t - B_s \sim \mathcal{N}(0, t - s)$
3. B_t is continuous in t almost surely (a.s.)
4. $B_0 = x$ a.s. for some known arbitrary value x.

It is clear these properties ensure that BM is tractable and easy to use. For instance, the independence and normal distribution of its increments causes BM to be Markovian and a martingale so that implementation using Monte Carlo methods is straightforward. In addition, its complexity is further reduced by being a continuous process.

Most of these useful properties inherent in BM are lost when it is generalised to fBM. This is since a new parameter, the Hurst parameter, denoted as H is introduced, where $H \in (0, 1)$. The Hurst parameter fundamentally influences how the fBM behaves; for instance, when $H \neq \frac{1}{2}$, fBM is not Markovian and does not have finite quadratic variation implying that it is not a semimartingale. To more accurately describe fBM and reflect its associated features, a combination of the

definitions of fBM from Mandelbrot and Van Ness (1968) and Nourdin (2012) is outlined:

Definition 2.2. (Fractional Brownian Motion) The random function $B_H(t,\omega) \triangleq B_t^H$ is called *fractional Brownian motion* with Hurst parameter $H \in (0,1)$. For $t > 0$, B_t^H is defined by

$$B_t^H = \frac{1}{\Gamma(H+\frac{1}{2})} \int_{-\infty}^{t} (t-s)^{H-1/2} dB_s,$$

where $(t-s)^{H-1/2}$ is called the *power-law kernel* . Furthermore, it has covariance structure

$$\mathbb{E}\left[B_t^H B_s^H\right] = \tfrac{1}{2}(t^{2H} + s^{2H} - |t-s|^{2H}).$$

Definition 2.2 shows that fBM is in fact a fractional integral with respect to the standard BM process. A brief summary of fractional calculus providing the necessary tools for methods in this paper can be found in Section A.1 of Appendix A. In addition, it is observed that fBM is non-Markovian because of the power-law kernel. This holds since for $H \neq \frac{1}{2}$, the integrand is always a function of t and so an increment of fBM, say $B_{t_2}^H - B_{t_1}^H$ for $t_2 > t_1$, can never be independent of $\mathcal{F}_{t_1}$. It also has stationary increments which implies that $B_{t_2}^H - B_{t_1}^H \sim B_{t_2-t_1}^H$. This can be seen from its covariance structure for $\mathbb{E}[(B_{t_2}^H - B_{t_1}^H)^2]$, since if the squared term is expanded, the expression simplifies to $\mathbb{E}[(B_{t_2-t_1}^H)^2]$. When assessing different Hurst parameter values, notice for $H = \frac{1}{2}$ that standard BM is obtained. For $H < \frac{1}{2}$, it can be shown, for instance in Shevchenko (2014), that the covariance of non-intersecting fBM increments is negative, whereas for $H > \frac{1}{2}$, the covariance is positive. FBM also is nowhere differentiable, and displays self-similarity and time-inversion properties. These properties, although not stated here, can be found in sources such as Nourdin (2012) and Shevchenko (2014).

2.2 Empirical Evidence for Fractional Brownian Motion

Historically, fBM was used in stock price modelling with the intention of creating more realistic dynamics. This was largely because the Hurst parameter in fBM allowed autocorrelation dynamics to be included in the models. For instance, since the positive autocorrelation of share price returns is considered a stylised feature of share behaviour, an fBM model assuming that $H > \frac{1}{2}$ would capture this feature. However, research such as that in Rogers (1997) concluded that arbitrage was admitted for $H > \frac{1}{2}$ since an equivalent martingale measure (EMM) could not exist under this condition.

Given the inability of fBM stock price models to construct arbitrage-free prices, its usefulness in stock price modelling was negated. However, a resurgence in the

popularity of fBM occurred as it became more and more studied as to its implementation in volatility modelling. An aforementioned pioneering paper performing such research by Gatheral *et al.* (2018) shows substantial empirical evidence for the rough behaviour of market volatility.

To begin, Gatheral *et al.* (2018) investigate the term structure of at-the-money (TS ATM) implied volatility (IV) skew of the S&P Index. This is defined as

$$\psi(\tau) := \left| \frac{\partial}{\partial k} \sigma_{BS}(k, \tau) \right|_{k=0},$$

where k is the log-moneyness of the option and τ the term to maturity, and indicates how the Black-Scholes IV varies for ATM options with term to maturity. Their result demonstrates that the TS ATM skew explodes at very short terms to maturity, and that it fits a power-law function very well (Figure 2.1). Indeed, this power-law fit is further corroborated in Fouque *et al.* (2004), and it is theoretically demonstrated in Fukasawa (2011) that this fit implies fBM dynamics.

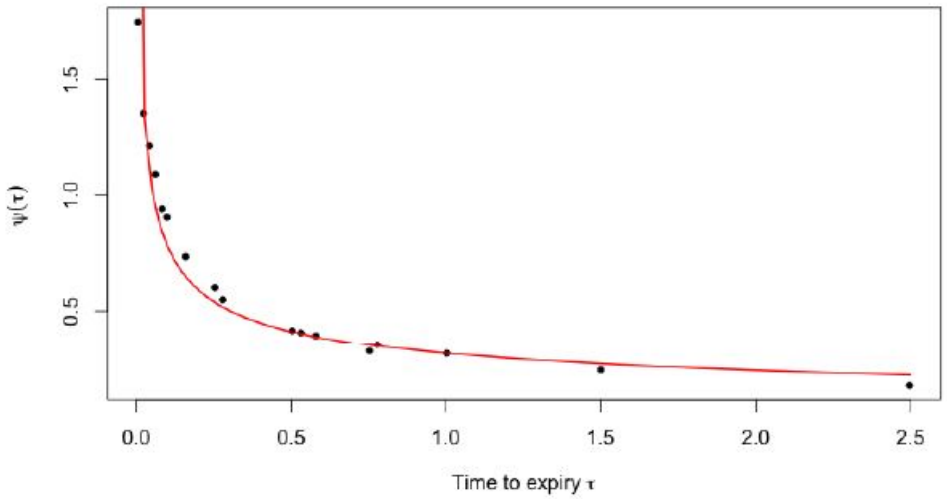

Fig. 2.1: The S&P ATM volatility skew as of June 20, 2013; reproduced from Gatheral *et al.* (2018). The black dots represent the non-parametric estimates, and the red curve represents the power-law fit $\psi(\tau) = A\tau^{-0.4}$.

Fouque *et al.* (2004) make use of a fast mean-reversion asymptotic approach which is utilised to capture the influence of volatility on derivative prices. It requires that the observed implied volatility $\sigma_{BS}(k, \tau)$ surface be fitted to an affine function of

log-moneyness-to-maturity ratio (LMMR) specified as follows:

$$\sigma_{BS}(k,\tau) = a \times \text{LMMR} + b \tag{2.1}$$
$$\text{LMMR} = \frac{k}{\tau},$$

where k and τ are specified as before. It is concluded for the S&P IV surface that the term structure is not τ^{-1} as in the LMMR variable, but rather that it is τ^{-q}, for some $q \approx \frac{1}{2}$.

Similarly, Fukasawa (2011) shows that IV can be transformed using the Edgeworth expansion for diffusions. Performing this expansion yields the affine structure that is seen in Equation (2.1). It is concluded that for a stochastic volatility model driven by fBM, the TS ATM volatility skew has the form of a power-law function $\psi(\tau) \sim \tau^{H-1/2}$, where H is the Hurst parameter.

2.3 Testing the Hurst Parameter

Using the power-law relationship $\psi(\tau) \sim \tau^{H-1/2}$ posited in Section 2.2, Gatheral *et al.* (2018) test the viability of the Hurst parameter values implied from market data. This is done by assessing the log-volatility of the NASDAQ, S&P, DAX and Bund futures with a measure called the microstructure noise index developed by Rosenbaum (2011).

The microstructure noise index is in fact an extension of the traditional signature plot measure defined as

$$P = \sum_{n=1}^{N} |\log(\sigma_{n\Delta}) - \log(\sigma_{(n-1)\Delta})|^2,$$

where Δ is the mesh size which represents the minimum waiting time until new data can be recorded. The size of Δ can vary, but is equal to one second for the data used in Rosenbaum (2011). Intuitively, if P is multiplied by $\frac{1}{N}$ and $N \to \infty$, the signature plot becomes the quadratic variation which gives some measure of the microstructure noise that is present. This is simultaneously a drawback in that the measure implicitly assumes viability only for semimartingale processes. To overcome this drawback by creating a measure that works for non-semimartingale processes, Rosenbaum (2011) extends the signature plot measure to a q-norm; and this results in the microstructure noise index being obtained. To perform this extension, a Besov smoothness space, a generalisation of a Sobolev space, must be effected. It is notated as $\mathcal{B}^s_{q,p}$ for some $s > 0$ and $1 \leq q, p \leq \infty$; and, intuitively, is a space that ensures regularity and convergence properties for its constituent vectors by quantifying its order of smoothness (Rosenbaum, 2009). To a certain extent, this acts also

as a criterion of differentiability. Given that this space indicates smoothness/differentiability for its constituent vectors, it is plausible that it measures the "noisiness" of these vectors. By effecting the Besov smoothness space, the microstructure noise index is observed to be

$$Nm(q,\Delta) = \sum_{n=1}^{N} |\log(\sigma_{n\Delta}) - \log(\sigma_{(n-1)\Delta})|^q, \tag{2.2}$$

where the N on the left-hand side (LHS) is the maximum number of partitions for mesh Δ. Additionally, Rosenbaum (2011) shows that Equation (2.2) converges asymptotically for a fBM with Hurst parameter H implying that the sample paths of the fBM belong to $\mathcal{B}^H_{q,\infty}$ a.s. It is also found that H is independent of the q chosen.

To analyse the market implied Hurst parameter values, Gatheral *et al.* (2018) observe that dividing by N on both sides of Equation (2.2) and then taking $N \to \infty$ would yield the expectation of the log-volatility increments, provided two conditions are met. The first is that the increments are stationary, and the second is that the necessary convergence properties hold as $N \to \infty$. As seen in Section 2.1, the increments of fBM are indeed stationary, and so the first requirement is satisfied. The second condition is satisfied because of the asymptotic convergence of fBM in $\mathcal{B}^H_{q,\infty}$ which, by the weak law of large numbers, implies that $m(q,\Delta)$ converges to its expectation. Given the convergence of $m(q,\Delta)$ under these conditions, Gatheral *et al.* (2018) propose for the various market observed volatilities that

$$m(q,\Delta) \to \mathbb{E}\left[|B^H_{t+\Delta} - B^H_t|^q\right] = K_q \Delta^{qH}, \tag{2.3}$$

where $m(q,\Delta)$ is as seen in (2.2), B^H_t is a fBM with Hurst parameter H, and K_q is the q^{th} moment of B^H_t. If Equation (2.3) holds, then $\log m(q,\Delta)$ would yield an affine relationship of the form $\zeta_q \log \Delta + \log K_q$, where the slope is expected to be $\zeta_q \sim qH$. Plotting $\log m(q,\Delta)$ against $\log \Delta$ for different increments of Δ could test this affine relationship, and the associated Hurst parameter could be determined from the slope $\zeta_q \sim qH$. This is done in Gatheral *et al.* (2018) by proxying daily spot variances by daily realized variance estimates over 3,540 trading days from January 3, 2000 to March 31, 2014. The associated $\log m(q,\Delta)$ against $\log \Delta$ plots for the S&P index are presented below. The gradients displayed in Figure 2.2 for different values of q are approximately similar which validates the independence of q and H. Then, using the relationship $\zeta_q \sim qH$ and plotting q against ζ_q, it can be seen that a value of $H = 0.142$ fits very well (Figure 2.3). Overall, these plots provide very strong empirical evidence for the existence of fBM in the market volatility. Importantly, given the evidence that the H values determined from the data are all less than $\frac{1}{2}$, the stylised notion of the slow decay of the autocorrelation of the volatility, also called long memory, is contradicted (Gatheral *et al.*, 2018).

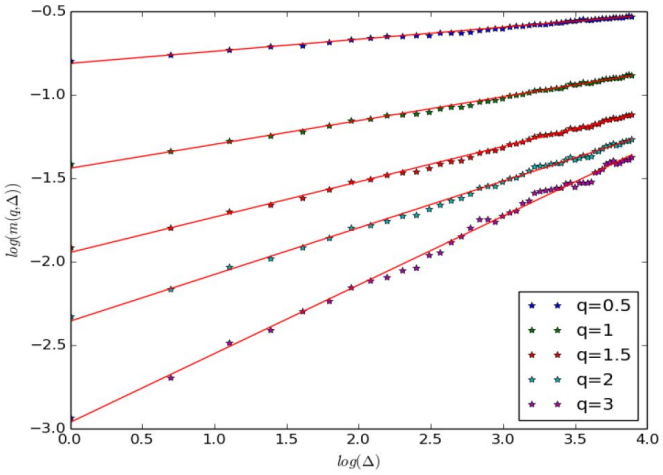

Fig. 2.2: $\log m(q, \Delta)$ as a function of $\log \Delta$, for the S&P Index; reproduced from Gatheral *et al.* (2018).

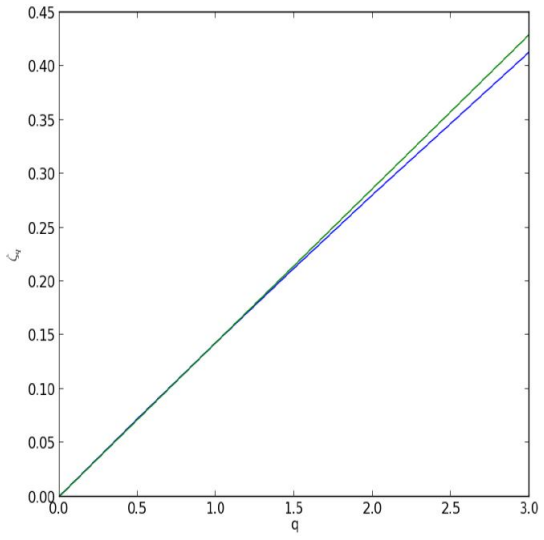

Fig. 2.3: ζ_q (blue) and $0.142 \times q$ (green), for the S&P Index; reproduced from Gatheral *et al.* (2018).

Chapter 3

Modelling Under Rough Volatility

3.1 The Rough Heston

To incorporate volatility smile/skew dynamics in option pricing, the classical Heston (1993) stochastic volatility model is often chosen. Given that the Cox-Ingersoll-Ross volatility dynamics of the classical Heston (cHeston) contains ordinary BM, one would naturally expect that there is some way to extend this by using fBM instead. It is shown in El Euch and Rosenbaum (2019) that this, in fact, is possible and results in a generalised version of the cHeston called the rough Heston (rHeston). Moreover, a characteristic function (CF) of the rHeston can also be derived. Before the rHeston is considered, a derivation of the cHeston CF will be presented as this provides the necessary intuition to extend it to the fBM equivalent.

3.1.1 Deriving Classical Heston

The classical model of Heston (1993) can be derived from the share price and volatility dynamics

$$\begin{aligned} dS_t &= S_t\sqrt{V_t}dW_t \\ dV_t &= \gamma(\theta - V_t)dt + \gamma\nu\sqrt{V_t}dB_t \ , \end{aligned} \tag{3.1}$$

with correlated Brownian motions $d[W,B]_t = \rho dt$, and $\gamma, \theta, \nu, V_0 > 0$. Note that (3.1) uses the model specification as presented in El Euch and Rosenbaum (2019), and excludes the short rate parameter by using the numeraire deflated process to simplify the derivation. With regards to parametrization, it is common to let $\gamma\nu = \sigma$ so that the σ parameter represents the volatility of the variance. It is easy to see that dynamics (3.1) have finite quadratic variation implying that they are semimartingales. Additionally, the dynamics are Markovian since they depend only on S_t and V_t.

To begin the derivation of the cHeston CF, it is required that some function resembling the CF given dynamics (3.1) is defined. Hence, let

$$L(u, a, V_u, S_u) = \mathbb{E}\left[e^{ia \log S_t} \middle| \mathcal{F}_u\right]$$

for some terminal time t, and let $L_u = L(u, a, V_u, S_u)$ for brevity. It can be seen that L_u is the CF written in the form of an expectation. Furthermore, L is a martingale since for times $u_2 > u_1$ and letting $X = e^{ia \log S_t}$,

$$\mathbb{E}[L_{u_2}|\mathcal{F}_{u_1}] = \mathbb{E}\Big[\mathbb{E}[X|\mathcal{F}_{u_2}]\Big|\mathcal{F}_{u_1}\Big] = \mathbb{E}[X|\mathcal{F}_{u_1}] = L_{u_1}$$

by using the Tower Property of conditional expectation. To proceed, the Feynman-Kač theorem can be utilised on L_u as in El Euch and Rosenbaum (2019). However, it is more intuitive to note that the martingale structure of L_u implies that its drift terms must be zero. Therefore, using the multivariate extension of Itô's Formula on function $L = L(u, a, V, S)$ and equating the dt terms to zero, the following partial differential equation (PDE) is obtained:

$$\partial_t L + \gamma(\theta - V)\partial_v L + \tfrac{1}{2}S^2 V \partial^2_{ss} L + \tfrac{1}{2}(\gamma\nu)^2 V \partial^2_{vv} L + \rho\gamma\nu S V \partial^2_{sv} L = 0, \tag{3.2}$$

with a terminal condition $L(t, a, V^*, S^*) = \mathbb{E}\left[e^{ia \log S^*}\middle|\mathcal{F}_t\right] = e^{ia \log S^*}$ for $S_t = S^*$ and $V_t = V^*$. This PDE implicitly describes the structure of the cHeston CF, since the derived CF substituted into (3.2) must equal zero. By using $\mathbb{E}\left[e^{iaX_{t-u}}|\mathcal{F}_u\right]$ for $X_{t-u} = \log \frac{S_t}{S_u}$ and a "guessed" solution as seen in Heston (1993), a viable CF can be found. This is written as

$$\mathbb{E}\left[e^{iaX_{t-u}}\middle|\mathcal{F}_u\right] = \mathbb{E}\left[e^{ia \log S_t}\middle|\mathcal{F}_u\right] e^{-ia \log S_u} = \exp\big(g(a, t-u) + V_u h(a, t-u)\big),$$

where the exponential term on the RHS is the "guessed" form of the solution. When the time variable $u = 0$, the expectation becomes $\mathbb{E}\left[e^{iaX_t}\right]$ which is the form desired to derive the CF. Then, the solutions of $g(a, t)$ and $h(a, t)$ will completely describe this CF. Note also that the time component for g and h are defined with respect to term to maturity. By putting $t = 0$ also, it can be seen that the implied initial conditions are $g(a, 0) = h(a, 0) = 0$.

The above equation can now be rewritten in terms of L_u so that relationship described by PDE (3.2) can be used to solve for $g(a, t)$ and $h(a, t)$. This yields

$$L(u, a, S_u, V_u) = \mathbb{E}\left[e^{ia \log S_t}\middle|\mathcal{F}_u\right] = \exp\big(g(a, t-u) + V_u h(a, t-u) + ia \log S_u\big), \tag{3.3}$$

and consequently the partial derivatives for function $L(u, a, S, V)$ implied from

PDE (3.2) are

$$\begin{aligned} &\partial_t L = -(\partial_t g + V\partial_t h)L \quad \forall u \in [0,t], && \partial^2_{sv} L, = \tfrac{iah}{S} L, \\ &\partial_v L = hL, && \partial^2_{vv} L = h^2 L, \\ &\partial_s L = \tfrac{ia}{S} L, && \partial^2_{ss} L = \tfrac{ia(ia-1)}{S^2} L, \end{aligned}$$

where $\partial_t L$ is calculated using the Chain Rule. Using the PDE, putting $u = 0$ and dividing through by L, the following is obtained:

$$-\partial_t g - V\partial_t h + \gamma(\theta - V)h + \tfrac{1}{2}Via(ia-1) + \tfrac{1}{2}\gamma^2\nu^2 V h^2 + \rho\gamma\nu V iah = 0.$$

Grouping the V terms and taking them to the RHS, it is seen that

$$\begin{aligned} &-\partial_t g + \gamma\theta h = \Psi V, \\ &\quad \text{where} \;\; \Psi = \partial_t h + \gamma h - \tfrac{1}{2}ia(ia-1) - \tfrac{1}{2}\gamma^2\nu^2 h^2 - \rho\gamma\nu iah. \end{aligned}$$

Since V is arbitrary, the only way the equation can hold is if the LHS equals zero and if $\Psi = 0$. This implies that the solution to the CF is defined by solving the Riccati ODE

$$\partial_t h = -\tfrac{1}{2}(a^2 + ia) + \gamma(\rho\nu ia - 1)h + \tfrac{(\gamma\nu)^2}{2}h^2, \quad h(a,0) = 0, \tag{3.4}$$

and by solving the LHS part

$$\partial_t g = \gamma\theta h \iff g(a,t) = \gamma\theta \int_0^t h(a,s)ds, \quad g(a,0) = 0. \tag{3.5}$$

To solve 3.4, a general solution can be applied, for which its derivation is found in part A.2 of the Appendix. Rewriting this as $\partial_t h = Ah^2 + Bh + D$, and using the general solution from Equation (A.3), the Riccati ODE can be solved with

$$h = \frac{\omega'}{a\omega},$$

for $\omega = C_1 e^{x_+ t} + C_2 e^{x_- t}$, where x_+ and x_- are the roots of the auxiliary polynomial $p = x^2 - Bx + AD$. Therefore, $x_\pm = \frac{1}{2}\left(B \pm \sqrt{B^2 - 4AD}\right)$. Note that ω must also be a variable of the term to maturity, so it follows that:

$$\omega' = -C_1 x_+ e^{x_+ t} - C_2 x_- e^{x_- t}$$

so that the initial condition $h(a,0) = 0$ gives

$$\omega' = 0 = -C_1 x_+ - C_2 x_- \Rightarrow C_1 = -C_2 \frac{x_-}{x_+}.$$

Substituting C_1 into ω and ω', and then these into the general solution of h, the following is obtained:

$$\begin{aligned} h &= \frac{C_2 x_- \left(e^{x_- t} - e^{x_+ t}\right)}{AC_2 \left(e^{x_- t} - \frac{x_-}{x_+} e^{x_+ t}\right)} \\ &= \frac{\left(1 - e^{(x_+ - x_-)t}\right) \frac{x_-}{A}}{1 - \frac{x_-}{x_+} e^{(x_+ - x_-)t}}, \end{aligned}$$

and from here it is easy to manipulate this into the form

$$h(a,t) = \frac{(1 - e^{-mt})x^-}{1 - ne^{-mt}}$$

for the parameters m and n as seen in Part A.3 of the Appendix. What remains is to find $g(a,t)$ which involves integrating $h(a,t)$. Hence

$$\int_0^t h(a,s)ds = \int_0^t \frac{(1 - e^{-ms})x^-}{1 - ne^{-ms}} ds$$

must be determined. A substitution $u = e^{-ms}$ can be used to simplify the expression. This also implies $ds = \frac{-1}{mu} du$. The integral is hence equivalent to

$$\int_0^t h(a,s)ds = \frac{x^-}{m} \int_1^{e^{-mt}} \frac{u-1}{u(1-nu)} du.$$

Then, using partial fractions, it is found that

$$\frac{u-1}{u(1-nu)} = \frac{A}{u} + \frac{B}{1-nu} = \frac{A(1-nu)}{u(1-nu)} + \frac{Bu}{u(1-nu)}$$

so that the numerator is $(B - An)u + A$. This must equal $u - 1$ from the numerator on the LHS, so by inspection, it is seen that $A = -1$ and $B = 1 - n$. As a result, the integral becomes

$$\begin{aligned} \int_0^t h(a,s)ds &= \frac{x^-}{m} \int_1^{e^{-mt}} \frac{-1}{u} du + \frac{x^-}{m} \int_1^{e^{-mt}} \frac{1-n}{1-nu} du \\ &= \frac{x^-}{m} \Big[-\log u \Big|_1^{e^{-mt}} + \frac{x^-}{m} \left[\frac{1-n}{-n} \log(1-nu) \right] \Big|_1^{e^{-mt}} \\ &= x^- t - \frac{x^-}{m} \frac{1-n}{n} \log\left(\frac{1 - ne^{-mt}}{1-n} \right). \end{aligned}$$

Now, notice that

$$\begin{aligned} x^- \frac{1-n}{n} &= x^- \left(\frac{1}{n} - 1 \right) = x^- \left(\frac{x^+}{x^-} - 1 \right) = x^+ - x^- \\ &= \tfrac{1}{v} \sqrt{b^2 - 4vc} = \tfrac{1}{v} m. \end{aligned}$$

Using these results, it can be seen that

$$g(a,t) = \int_0^t h(a,s)ds = \gamma\theta\left(x^- t - \frac{1}{v}\log\left\{\frac{1-ne^{-mt}}{1-n}\right\}\right). \tag{3.6}$$

This is exactly the same as that shown in A.3, except in this case, the short rate is zero, so that that term does not feature in $g(a,t)$. Furthermore, this is consistent for the initial condition $g(a,0) = 0$.

3.1.2 Deriving Rough Heston

The rHeston dynamics can intuitively be seen as an extension of the cHeston volatility dynamics (3.1) to its rough equivalent. These dynamics are as follows:

Definition 3.1. (Rough Heston Model) A stochastic volatility process with dynamics

$$\begin{aligned} dS_t &= S_t\sqrt{V_t}dW_t \\ V_t &= V_0 + \tfrac{1}{\Gamma(H+1/2)}\int_0^t (t-s)^{H-1/2}\gamma(\theta - V_s)ds + \tfrac{1}{\Gamma(H+1/2)}\int_0^t (t-s)^{H-1/2}\gamma\nu\sqrt{V_s}dB_s \end{aligned} \tag{3.7}$$

is called Rough Heston, where the parameters $\gamma, \theta, \nu, V_0 > 0$, W_t and B_t are correlated BMs with $d[W,B]_t = \rho\, dt$ and Hurst parameter $H \in (0, \frac{1}{2})$.

This intuitive relationship between the cHeston and rHeston is not sufficient to prove that these rHeston dynamics hold, but at least provides some motivation for their viability. Furthermore, it conceals the difficulty of a rigorous derivation since it ignores the fact that the volatility process is neither a semimartingale nor Markovian. By implication, a rigorous derivation cannot use Itô's Lemma to solve for the volatility as was done for the cHeston case in Section 3.1, and so a different approach must be taken. El Euch and Rosenbaum (2019) instead consider modelling volatility at discrete times, and then find the continuous-time dynamics by observing the convergence of this model. The model chosen is the nearly unstable Hawkes process since, given the assumptions of high endogeneity of market transactions and "no statistical arbitrage" mechanisms, it can realistically model the market microstructure. Then, by proving convergence of this model over infinitesimal intervals, El Euch and Rosenbaum (2019) show that it converges to the rHeston dynamics (3.7). Additionally, it is shown that the rHeston dynamics are in fact well-defined and that the necessary Hölder regularity conditions hold. Lastly, the cHeston dynamics are obtained if $H = \frac{1}{2}$, and this shows that the rHeston is in fact a generalisation of the cHeston dynamics.

Given these rHeston dynamics, a corresponding rHeston CF which generalises the cHeston CF can also be derived. This is proven in El Euch and Rosenbaum (2019) and forms the basis of the techniques used to price options with fractional volatility dynamics which will be seen in Chapter 4. Prior to stating this theorem, the necessary fractional calculus definitions are provided:

Definition 3.2. (Fractional Operators) The *fractional integral* of a function $f(x)$ is defined as

$$I^{\alpha}f(x) = \frac{1}{\Gamma(\alpha)}\int_0^x (x-t)^{\alpha-1}f(t)dt.$$

In a similar vain, the *fractional derivative* is defined as

$$D^{\alpha}f(x) = \frac{1}{\Gamma(\alpha-1)}\frac{d}{dt}\int_0^x (x-t)^{-\alpha}f(t)dt.$$

Notationally, it is implied that $I^{\alpha} = D^{-\alpha}$ and $I^{-\alpha} = D^{\alpha}$. Of course, it is trivial for some function $f(a,t)$ that $I^{\alpha}D^{\alpha}f(a,t) = f(a,t)$, and likewise that $I^{1-\alpha}f(a,t) = I^{1}D^{\alpha}f(a,t)$.

Using the notation from Definition 3.2, the most crucial theorem of this paper proven in El Euch and Rosenbaum (2019) is stated as follows:

Theorem 3.3. ***(Rough Heston Characteristic Function)*** *Consider the rough Heston model (3.7) with a correlation between the two BMs ρ satisfying $\rho \in \left(-\frac{1}{\sqrt{2}}, \frac{1}{\sqrt{2}}\right]$. For all $T \geq 0$ and a fixed $a \in \mathbb{R}$, we have the characteristic function of the log stock price*

$$\phi(a,T) = \exp\left(\theta\gamma I^{1}h(a,T) + V_0 I^{1-\alpha}h(a,T) + ia\log S_0\right), \tag{3.8}$$

where $h(a,\cdot)$ is the solution of the fractional Riccati equation

$$D^{\alpha}h(a,t) = \tfrac{1}{2}(-a^2-ia)+\gamma(ia\rho\nu-1)h(a,t)+\tfrac{1}{2}(\gamma\nu)^2h^2(a,t), \quad I^{1-\alpha}h(a,0) = 0, \tag{3.9}$$

with initial condition $h(a,0) = 0$, which admits a unique continuous solution . Additionally, $\alpha = H + \frac{1}{2}$.

Referring to Appendix A.3, it is possible to see that the rHeston CF generalises the cHeston CF, since if $\alpha = 1$ for the rHeston CF (3.8), then the cHeston CF is obtained. Additionally, both the cHeston and rHeston CF are completely defined once function $h(a,T)$ has been found by solving its corresponding ODE. This leads to one of the major differences between the classical and rough case. Even though the structure of the rough Riccati ODE (3.9) is exactly the same as that of the classical Riccati ODE (3.4), the rough case requires that it is solved to the fractional order. Hence, to determine the rHeston CF requires that numerical techniques to solve fractional ODEs must be utilised.

3.1.3 Solving Fractional ODEs

To determine $y(t) = h(a,t)$ in the rough Heston CF, it is wished that fractional ODEs of the form $D^{\alpha}y(t) = f(t, y(t))$, with initial condition $y(0) = y_0$ are to be solved. This equates to finding $y(t)$ as represented by a Volterra integral equation (Diethelm *et al.*, 2002); that is,

$$y(t) = \sum_{k=0}^{\lceil\alpha\rceil-1} y_0^{(k)} \frac{t^k}{k!} + \frac{1}{\Gamma(\alpha)} \int_0^t (t-u)^{\alpha-1} f(u, y(u)) du. \tag{3.10}$$

Note that this is a generalisation of the problem specification for standard ODEs of first order; i.e., if $\alpha = 1$, a standard first order ODE is obtained with the additional caveat that the implied initial condition is $y_0 = 0$. As already seen in Section 2.3, the Hurst parameters considered in market data and for the rough Heston model (3.7) are $H = (0, \frac{1}{2})$, which implies that $\lceil\alpha\rceil = 1$ for the purposes of solving fractional ODE (3.9). This means that the summation term in (3.10) disappears, so that the Volterra integral equation simplifies to

$$y(t) = \frac{1}{\Gamma(\alpha)} \int_0^t (t-u)^{\alpha-1} f(u, y(u)) du. \tag{3.11}$$

An important difference between fractional differential operators and standard differential operators is that the fractional case has non-local structure (Diethelm *et al.*, 2002). This means that in general for $D^{\alpha}y(t) = f(t, y(t))$, that the integral depends on all of the values over the range $[0, t]$ implying that the Fundamental Theorem of Calculus cannot be used to simplify the numerical methods utilised. For instance, $y(t_2) - y(t_1) \neq \int_{t_1}^{t_2} f^*(u, y(u)) du$ for $f^*(u, y(u)) = \Gamma(\alpha)^{-1}(t_2 - u)^{\alpha-1} f(u, y(u))$, and so the fractional integral cannot depend only on values over $[t_1, t_2]$ as for generic ODE numerical schemes. This needs to be acknowledged when determining solutions.

It is often the case that fractional ODEs do not have analytical solutions, and so numerical schemes are required to solve them. Three different numerical methods will be considered, namely standard quadrature, quadrature for products, and the fractional Adams scheme (El Euch and Rosenbaum, 2019). These are listed in increasing order of implementational difficulty which hence also implies increasing order of accuracy. As a consequence, the fractional Adams scheme which is developed and studied in Diethelm *et al.* (2002) is the method chosen for solving fractional Riccati ODE (3.9) and for implementation in Chapter 4. To develop the necessary intuition for deriving these three methods, the Adams-Bashforth-Moulton (ABM) Algorithm for solving standard ODEs presented in Diethelm *et al.* (2002) is first considered. The three methods to solve fractional Riccati ODE (3.9) are then derived and implemented.

Adams-Bashforth-Moulton Algorithm

The ABM algorithm is used to solve first-order ODEs of the form $Dy(t) = f(t, y(t))$, with initial condition $y(0) = y_0$. Assume that some uniform grid $\{t_n = nh \mid n = 0, 1, ..., N\}$ for $N \in \mathbb{N}$ and $h := T/N$ is used. This method is recursive since the n^{th} approximation is required to calculate the $n + 1^{\text{th}}$ approximation. Supposing that approximations $\hat{y}(t_j) \approx y(t_j)$ for $j = 1, 2, ..., n$ have all been calculated, then $\hat{y}(t_{n+1})$ is calculated by using the fact that

$$y(t_{n+1}) = y(t_n) + \int_{t_n}^{t_{n+1}} f(u, y(u))du, \tag{3.12}$$

and subsequently replacing the integral of (3.12) with an approximation based on some interpolation function that is used to make an assumption on how the values of $f(u, y(u))$ for $u \in [t_n, t_{n+1}]$ behave. For example, the well known two-point trapezoidal quadrature formula

$$\int_a^b g(u)du \approx \frac{b-a}{2}\big(g(a) + g(b)\big)$$

is derived by making the assumption that the $g(u)$ values for $u \in [t_n, t_{n+1}]$ can be determined by linearly interpolating the points $g(a)$ and $g(b)$. This assumption about how $g(u)$ behaves over intervals is formalised as

$$g(u) \approx g^*(u) = \frac{b-u}{b-a}g(a) + \frac{u-a}{b-a}g(b), \quad u \in [a, b],$$

where $g^*(u)$ is called the piecewise linear interpolant of $g(u)$. Then, taking $\int_a^b g^*(u)du$ results in the two-point trapezoidal quadrature formula seen above, where its name comes from trapezium shape of the areas of the integrated intervals. Using this assumption and then replacing y values with known approximations $\hat{y}$ yields

$$\hat{y}(t_{n+1}) = \hat{y}(t_n) + \frac{h}{2}\big[f(t_n, \hat{y}(t_n)) + f(t_{n+1}, \hat{y}(t_{n+1}))\big], \tag{3.13}$$

where $h = (n + 1)h - nh = t_{n+1} - t_n$. This formulation, however, is problematic since $\hat{y}(t_{n+1})$ appears on both sides of equation (3.13) and cannot necessarily be factorised to give a single $\hat{y}(t_{n+1})$. This is since the function f need not be linear in general. To overcome this problem, a predictor approximation is introduced.

The predictor is a preliminary approximation of $y(t_{n+1})$ and is found by once again making an assumption about the behaviour of the function $f(u, y(u))$ between points in the mesh grid. By assuming that some arbitrary function $g(u)$ is constant over an interval $[a, b]$ results in some rectangle approximation rule. If it is assumed that $g(u) \approx g^*(u) = g(a)\ \forall u \in [a, b]$, then the well-known rectangle rule

approximation $\int_a^b g(u)du \approx (b-a)g(a)$ is obtained. Using this on the integral in (3.12), and then substituting in approximations $\hat{y}$ yields

$$\hat{y}^p(t_{n+1}) = \hat{y}(t_n) + hf(t_n, \hat{y}(t_n)),$$

where $\hat{y}^p(t_{n+1})$ is the predictor approximation for $\hat{y}(t_{n+1})$. The ABM approximation for $y(t_{n+1})$ can hence be determined by substituting $\hat{y}^p(t_{n+1})$ into the RHS of (3.13) to get

$$\hat{y}(t_{n+1}) = \hat{y}(t_n) + \frac{h}{2}\left[f(t_n, \hat{y}(t_n)) + f(t_{n+1}, \hat{y}^p(t_{n+1}))\right] \tag{3.14}$$

which concludes the derivation of the ABM algorithm.

Quadrature

When it comes to numerical approximations, the most simple and tractable approximation to implement is often that of the rectangle rule approximation that was seen in the derivation of the ABM predictor. Applying this to Volterra integral equation (3.11), the following approximation is derived:

$$\begin{aligned} y(t) &= \frac{1}{\Gamma(\alpha)} \int_0^t f^*(u, y(u))du \\ &= \frac{1}{\Gamma(\alpha)} \sum_{j=0}^{n-1} \int_{t_j}^{t_{j+1}} f^*(u, y(u))du \\ \Rightarrow y(t) &\approx \frac{1}{\Gamma(\alpha)} \sum_{j=0}^{n-1} (t_{j+1} - t_j) f^*(t_j, y(t_j)), \end{aligned}$$

where $f^*(u, y(u)) = (t-u)^{\alpha-1} f(u, y(u))$, and $t_j \in [0, t]\ \forall j = 0, 1, ..., n$. This method is used to solve equation (3.9), with its corresponding result displayed in Figure 3.1.

Overall, Figure 3.1 shows that a fairly good approximation is attained with very minimal effort. However, the trade-off of the simplicity shows in the accuracy of this method. Given the assumption of constant $f^*(u, y(u))$ values over intervals $[t_j, t_{j+1}]$, the approximations will result in concave functions always being underestimated and convex functions always being overestimated. It is hence unsurprising that the approximations in Figure 3.1 are larger than the solution which has convex shape. The accuracy can of course be improved by increasing the size of the mesh used (decreasing h), but this will trade efficiency and the computational power necessary.

Determining the degree of accuracy required for the problem at hand is crucial since each $\hat{y}(t_{n+1})$ depends on the previous $\hat{y}(t_n)$, and so the inaccuracies will

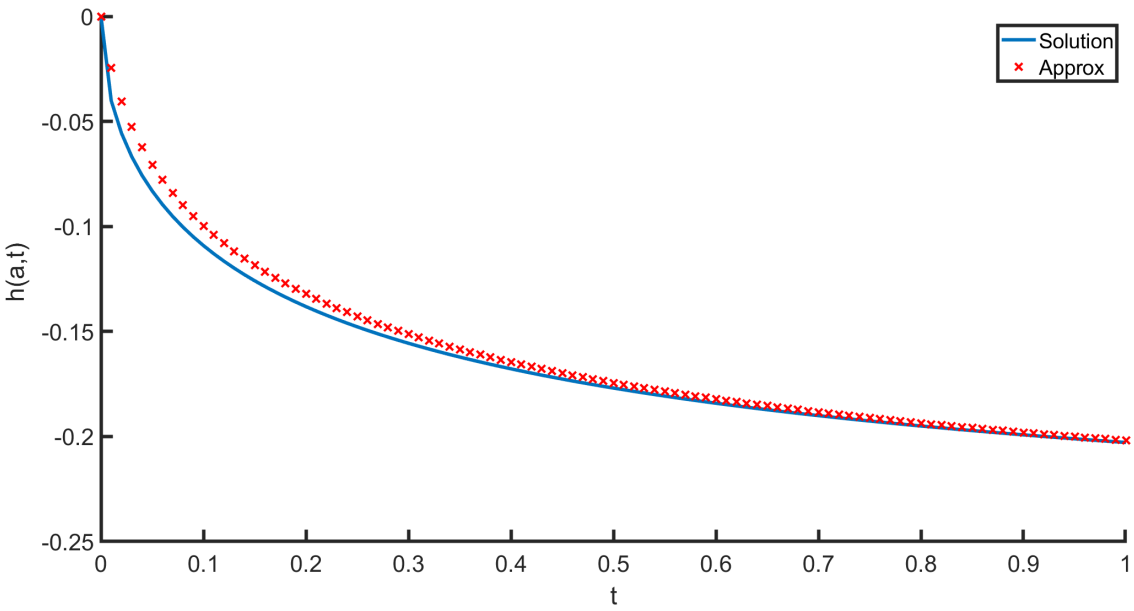

Fig. 3.1: Quadrature approximation for the real values of $D^\alpha h(a,t)$, for $\alpha = 0.55$, $a = 1$, and for equispaced nodes $t_j = t_0 + jh$, where $h = 0.01$ is chosen.

usually accumulate as n increases. For this example, it is not the case since the solution becomes flatter as t increases, so the assumption of constant $f^*(u, y(u))$ becomes more viable for larger t allowing the subsequent approximations to rectify. Hence, in some circumstances it may be acceptable to use rectangle quadrature, but it largely depends on the problem and also some experimentation.

Lastly, note that it is not possible to do a RHS quadrature approximation since the power-law kernel would explode at the last value in the mesh t_n. In general, this implies any quadrature approximations requiring $f^*(t_n, y(t_n))$ cannot be used. The LHS quadrature is hence viable since it truncates the integral to $[0, t_{n-1}]$, and prevents the power-law kernel from exploding.

Quadrature for Products

It was observed that the assumption of constant $f^*(u, y(u))$ values between intervals $[t_j, t_{j+1}]$ was one of the major sources of inaccuracy for the generic quadrature approximation. Additionally, the generic quadrature method above used the power-law kernel as part of the function $f^*(u, y(u))$, but the main function of interest is $D^\alpha y(u) = f(u, y(u))$. Hence, it seems intuitive that quadrature on $f^*(u, y(u))$ is inefficient given its use of the power-law kernel which provides no information on possible $y(u)$ values.

The quadrature for products approximation in Kythe and Puri (2011) tries to

account for these issues by separating $f(u, y(u))$ from the components independent of $y(u)$, say $g(u)$. Given it's independence of $y(u)$, the function $g(u)$ in the product function $g(u)f(u, y(u))$ is essentially that of some arbitrary scaling factor for $f(u, y(u))$. As a result, it is plausible that the quadrature approximations can be improved by leveraging the information that $g(u)$ provides on how $f(u, y(u))$ is scaled/weighted over certain intervals.

For the Volterra integral equation, deriving this method involves separating the power-law kernel from $f(u, y(u))$ by assuming that $f(u, y(u))$ is constant over intervals $[t_j, t_{j+1}]$. The scaling factor implied by the power-law kernel over this interval can then be determined. This results in an approximation of the form

$$\int_a^b g(u)f(u, y(u)) \approx \sum_{j=1}^{n} \omega(t_j)f(t_j, y(t_j)), \tag{3.15}$$

for $g(u) = (t-u)^{\alpha-1}$, $t_j \in [a, b]$ $\forall j \in \{1, 2, ...n\}$, and some weight function $\omega(u)$. This is actually a generalisation of rectangular quadrature approximation that has already been seen in the previous section. As is shown in Kythe and Puri (2011), by making the assumption that $f(u, y(u)) \approx f(a, y(a))$ $\forall u \in [a, b]$, the appropriate weight ω^* over this interval is observed to be

$$\int_a^b g(u)f(u, y(u))du \approx \left[\int_a^b g(u)\right] f(a, y(a)) = \omega^* f(a, y(a)). \tag{3.16}$$

Note that if it were the case that $g(u) = 1$, the original rectangle approximation $(b-a)f(a, y(a))$ would be obtained. In a similar way, the weights for the Volterra integral equation can then quite simply be derived as follows:

$$\begin{aligned}\int_{t_0}^{t_{n+1}} (t_{n+1}-u)^{\alpha-1}f(u, y(u))du &= \sum_{j=0}^{n} \int_{t_j}^{t_{j+1}} (t_{n+1}-u)^{\alpha-1}f(u, y(u))du \\ &\approx \sum_{j=0}^{n} b_{j,n+1}f(t_j, y(t_j)),\end{aligned} \tag{3.17}$$

where

$$\begin{aligned}b_{j,n+1} &= \int_{t_j}^{t_{j+1}} (t_{n+1}-u)^{\alpha-1}du = \tfrac{1}{\alpha}\left[(t_{n+1}-t_j)^{\alpha} - (t_{n+1}-t_{j+1})^{\alpha}\right] \\ &= \tfrac{h^{\alpha}}{\alpha}\left[(n-j+1)^{\alpha} - (n-j)^{\alpha}\right]\end{aligned} \tag{3.18}$$

using equispaced nodes $t_j = t_0 + jh$. Using this method to solve fractional Riccati ODE (3.9), the approximations shown in Figure 3.2 are obtained.

It can immediately be seen that the approximations attained here are far more accurate than that of the standard quadrature seen in Figure 3.1. Furthermore,

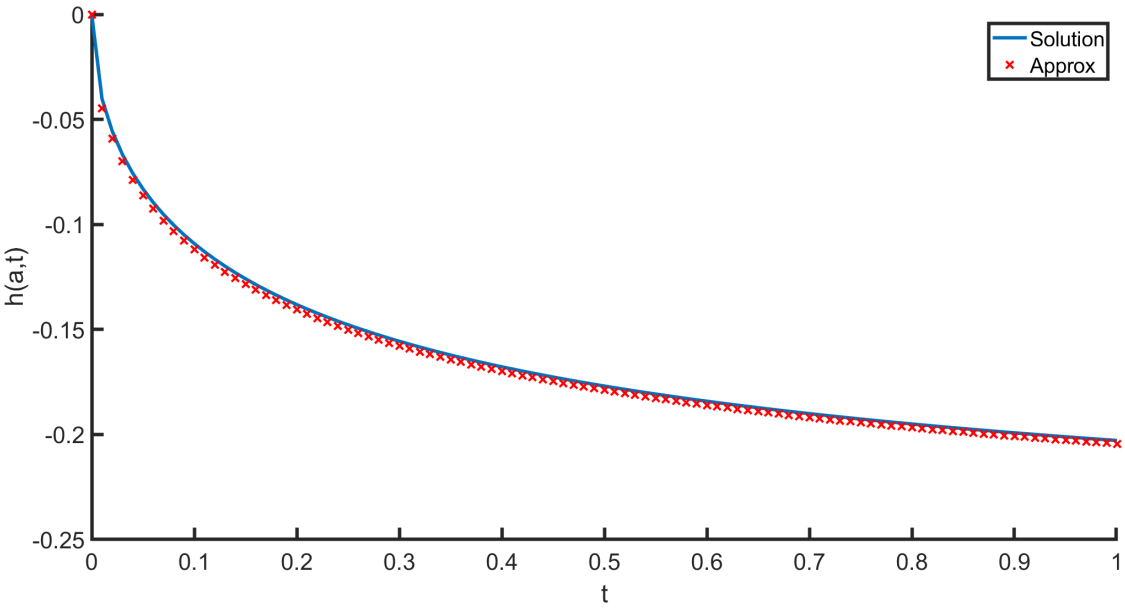

Fig. 3.2: Quadrature of products approximation for the real values of $D^{\alpha}h(a,t)$, for $\alpha = 0.55$, $a = 1$, and for equispaced nodes $t_j = t_0 + jh$, where $h = 0.01$ is chosen.

since the same mesh size is used as for the quadrature approximation, it can also be concluded that it is far more efficient. Given this large degree of accuracy, it can be asked why more precise approximations from the fractional Adam's method would be needed. Once again, this depends on the problem at hand. Since the rough Heston CF is to be used for pricing options, the most efficient and accurate answer is desired to ensure that the smallest possible approximation errors are accumulated for each successive $y(t_n)$.

An important caveat of this approximation, and in fact the fractional Adam's method also, is that it may not always be possible to implement since it is required that function $g(u)$ is integrated. However, for solving fractional ODEs, the integrability of the power-law kernel implies that it should always be possible to implement these approximations.

Fractional Adam's Algorithm

The derivation of the fractional Adam's algorithm is inspired from that of the ABM algorithm. Starting in a similar manner to the derivation of the ABM algorithm, some assumption about the behaviour of $f(u, y(u))$ in Volterra integral equation (3.11) must be made. For brevity, let $f(u)$ be the shorthand for $f(u, y(u))$, and define $I[f] = \int_0^{t_{n+1}} (t_{n+1} - u)^{\alpha-1} f(u)du$. It follows that assuming the behaviour of $f(u)$ between nodes $[t_{j-1}, t_j]$ amounts to deriving an approximation of the form

$I[f] \approx \sum_{j=0}^{n+1} a_{j,n+1} f(t_j)$ for corresponding weights $a_{j,n+1}$. In the ABM algorithm derivation, a piecewise linear interpolant was chosen which resulted in a two-point trapezoidal approximation for $y(t_{n+1})$. If a piecewise linear interpolant is chosen for fractional integrals; that is,

$$f(u) \approx f^*(u) = \frac{t_{j+1}-u}{t_{j+1}-t_j} f(t_j) + \frac{u-t_j}{t_{j+1}-t_j} f(t_{j+1}), \quad u \in [t_j, t_{j+1}),\ 0 \le j \le n, \tag{3.19}$$

the fractional Adam's scheme can be derived (Diethelm *et al.*, 2002). Applying this substitution and splitting the integral into a summation of intervals of the nodes gives the approximation:

$$\begin{aligned} I[f^*] = &\int_{t_0}^{t_1} (t_{n+1}-u)^{\alpha-1} \left[\frac{t_1-u}{t_1-t_0} f(t_0) + \frac{u-t_0}{t_1-t_0} f(t_1) \right] du \\ &+ \sum_{j=1}^{n-1} \int_{t_j}^{t_{j+1}} (t_{n+1}-u)^{\alpha-1} \left[\frac{t_{j+1}-u}{t_{j+1}-t_j} f(t_j) + \frac{u-t_j}{t_{j+1}-t_j} f(t_{j+1}) \right] du \\ &+ \int_{t_n}^{t_{n+1}} (t_{n+1}-u)^{\alpha-1} \left[\frac{t_{n+1}-u}{t_{n+1}-t_n} f(t_n) + \frac{u-t_n}{t_{n+1}-t_n} f(t_{n+1}) \right] du. \end{aligned}$$

This summation is split into these three intervals since this form shows that the $f(t_j)$ terms for $j \in \{1, 2, ..., n\}$ are repeated, whereas $f(t_0)$ and $f(t_{n+1})$ are not. For instance, letting $j = 1$, it can be seen that $f(t_1)$ appears in the integrals over $[t_0, t_1)$ and $[t_1, t_2)$ as follows:

$$\int_{t_0}^{t_1} (t_{n+1}-u)^{\alpha-1} \frac{u-t_0}{t_1-t_0} f(t_1) du + \int_{t_1}^{t_2} (t_{n+1}-u)^{\alpha-1} \frac{t_2-u}{t_2-t_1} f(t_1) du,$$

where the terms in front of the $f(t_1)$ are the only differences between the two integrals. Since the $f(t_j)$ values are known at nodes t_j, the $f(t_j)$ can be factored from the integral as was done in equation (3.16). This gives

$$\left[\int_{t_{j-1}}^{t_j} (t_{n+1}-u)^{\alpha-1} \tfrac{u-t_{j-1}}{t_j-t_{j-1}} du + \int_{t_j}^{t_{j+1}} (t_{n+1}-u)^{\alpha-1} \tfrac{t_{j+1}-u}{t_{j+1}-t_j} du \right] f(t_j) = a_{j,n+1} f(t_j),$$

for $0 \le j \le n+1$. Note that it is implied for $j = 0$ that the integral over $[t_{j-1}, t_j]$ is zero, and for $j = n+1$ that the integral over $[t_j, t_{j+1}]$ is zero also. This gives the representation seen in Diethelm and Freed (1998), where

$$a_{j,n+1} = \int_{t_0}^{t_{n+1}} (t_{n+1}-u)^{\alpha-1} \phi_{j,n+1}(u) du,$$

and

$$\phi_{j,n+1}(u) = \begin{cases} \frac{u-t_{j-1}}{t_j-t_{j-1}} & \text{if } t_{j-1} < u < t_j \\ \frac{t_{j+1}-u}{t_{j+1}-t_j} & \text{if } t_j < u < t_{j+1} \\ 0 & \text{otherwise.} \end{cases}$$

What remains is to solve for these weightings $a_{j,n+1}$ for the three cases over which the summation was split. These are $j = 0$, $j \in \{1, 2, ..., n\}$ and $j = n + 1$. In general, the following must be solved:

$$\begin{aligned} a_{j,n+1} &= \int_{t_{j-1}}^{t_j} (t_{n+1} - u)^{\alpha-1} \frac{u - t_{j-1}}{t_j - t_{j-1}} du + \int_{t_j}^{t_{j+1}} (t_{n+1} - u)^{\alpha-1} \frac{t_{j+1} - u}{t_{j+1} - t_j} du \\ &= \mathcal{I}_1 + \mathcal{I}_2. \end{aligned}$$

Integration by parts is required for both integrals, and gives

$$\begin{aligned} \mathcal{I}_1 &= \left[-\tfrac{1}{\alpha}(t_{n+1} - u)^{\alpha} \tfrac{u - t_{j-1}}{t_j - t_{j-1}} \right|_{t_{j-1}}^{t_j} + \int_{t_{j-1}}^{t_j} \tfrac{1}{\alpha}(t_{n+1} - u)^{\alpha} \tfrac{du}{t_j - t_{j-1}} \\ &= -\tfrac{1}{\alpha}(t_{n+1} - t_j)^{\alpha} - \left[\tfrac{1}{\alpha(\alpha+1)}(t_{n+1} - u)^{\alpha+1} \tfrac{1}{t_j - t_{j-1}} \right|_{t_{j-1}}^{t_j} \\ &= -\tfrac{1}{\alpha}(t_{n+1} - t_j)^{\alpha} - \tfrac{1}{\alpha(\alpha+1)} \tfrac{1}{t_j - t_{j-1}} \left[(t_{n+1} - t_j)^{\alpha+1} - (t_{n+1} - t_{j-1})^{\alpha+1} \right], \end{aligned}$$

and

$$\begin{aligned} \mathcal{I}_2 &= \left[-\tfrac{1}{\alpha}(t_{n+1} - u)^{\alpha} \tfrac{t_{j+1} - u}{t_{j+1} - t_j} \right|_{t_j}^{t_{j+1}} - \int_{t_j}^{t_{j+1}} \tfrac{1}{\alpha}(t_{n+1} - u)^{\alpha} \tfrac{du}{t_{j+1} - t_j} \\ &= \tfrac{1}{\alpha}(t_{n+1} - t_j)^{\alpha} + \left[\tfrac{1}{\alpha(\alpha+1)}(t_{n+1} - u)^{\alpha+1} \tfrac{1}{t_{j+1} - t_j} \right|_{t_j}^{t_{j+1}} \\ &= \tfrac{1}{\alpha}(t_{n+1} - t_j)^{\alpha} + \tfrac{1}{\alpha(\alpha+1)} \tfrac{1}{t_{j+1} - t_j} \left[(t_{n+1} - t_{j+1})^{\alpha+1} - (t_{n+1} - t_j)^{\alpha+1} \right]. \end{aligned}$$

Then, using equispaced nodes $t_j = t_0 + jh$, the three separate cases can be solved. For $j = 0$, note that $\mathcal{I}_1$ becomes zero. Hence:

$$\begin{aligned} a_{0,n+1} &= \tfrac{1}{\alpha}(t_{n+1} - t_0)^{\alpha} + \tfrac{1}{\alpha(\alpha+1)} \tfrac{1}{t_1 - t_0} \left[(t_{n+1} - t_1)^{\alpha+1} - (t_{n+1} - t_0)^{\alpha+1} \right] \\ &= \tfrac{1}{\alpha}(n+1)^{\alpha} h^{\alpha} + \tfrac{1}{\alpha(\alpha+1)} \tfrac{1}{h} \left[(nh)^{\alpha+1} - (n+1)^{\alpha+1} h^{\alpha+1} \right] \\ \Rightarrow a_{0,n+1} &= \tfrac{h^{\alpha}}{\alpha(\alpha+1)} \left[n^{\alpha+1} - (n - \alpha)(n+1)^{\alpha} \right]. \end{aligned}$$

For $j = n + 1$, note that $\mathcal{I}_2$ becomes zero. Hence:

$$\begin{aligned} a_{n+1,n+1} &= \tfrac{1}{\alpha(\alpha+1)} \tfrac{1}{t_{n+1} - t_n} (t_{n+1} - t_n)^{\alpha+1} \\ \Rightarrow a_{n+1,n+1} &= \tfrac{h^{\alpha}}{\alpha(\alpha+1)}. \end{aligned}$$

For $1 \leq j \leq n$, the sum of $\mathcal{I}_1$ and $\mathcal{I}_2$ is required. The following is obtained:

$$\begin{aligned} a_{j,n+1} &= \tfrac{1}{\alpha(\alpha+1)} \tfrac{1}{h} (t_{n+1} - t_{j+1})^{\alpha+1} - \tfrac{2}{\alpha(\alpha+1)} \tfrac{1}{h} (t_{n+1} - t_j)^{\alpha+1} \\ &\quad + \tfrac{1}{\alpha(\alpha+1)} \tfrac{1}{h} (t_{n+1} - t_{j-1})^{\alpha+1} \\ \Rightarrow a_{j,n+1} &= \tfrac{h^{\alpha}}{\alpha(\alpha+1)} \left[(n - j + 2)^{\alpha+1} - 2(n - j + 1)^{\alpha+1} + (n - j)^{\alpha+1} \right]. \end{aligned}$$

Substituting this approximation into Volterra integral equation (3.11) yields the first part of the fractional Adam's scheme:

$$\hat{y}(t_{n+1}) = \frac{a_{n+1,n+1}}{\Gamma(\alpha)} f(t_{n+1}, y(t_{n+1})) + \sum_{j=0}^{n} \frac{a_{j,n+1}}{\Gamma(\alpha)} f(t_j, \hat{y}(t_j)). \tag{3.20}$$

As with the ABM derivation, it is seen that $y(t_{n+1})$ appears on both sides of equation (3.20) and generally cannot be factorised. To overcome this, a predictor for the $y(t_{n+1})$ term in equation (3.20) is to be determined. This predictor can, in fact, be derived by using the quadrature of products method to yield the exact same result as Equation (3.18). This is rewritten for completeness:

$$\int_{t_0}^{t_{n+1}} (t_{n+1} - u)^{\alpha-1} f(u) du \approx \sum_{j=0}^{n} b_{j,n+1} f(t_j),$$
$$\text{where} \quad b_{j,n+1} = \tfrac{h^\alpha}{\alpha} \left[(n-j+1)^\alpha - (n-j)^\alpha\right]$$

using equispaced nodes. Using this approximation on Equation (3.11) yields the predictor

$$\hat{y}^p(t_{n+1}) = \sum_{j=0}^{n} \frac{b_{j,n+1}}{\Gamma(\alpha)} f(t_j, \hat{y}(t_j)), \tag{3.21}$$

and this completes the fractional Adam's method.

The solutions shown in Figures 3.1 and 3.2 are actually attained by using the fractional Adam's method since no analytical solution exists, and since it is the most accurate numerical solution discussed. Additional modifications of this algorithm are presented in Diethelm *et al.* (2002), but for the purposes of pricing options, this method is all that is required. Additionally, Appendix A.4 states the results of the derivation succinctly, whereas here it is written for the purpose of derivation and explanation. It must be noted that the weights written in Appendix A.4 include the $\Gamma(\alpha)$ terms. This means they are adjusted using the fact that $\Gamma(\alpha)\alpha(\alpha+1) = \Gamma(\alpha+2)$, but of course they amount to the same results as are derived here.

3.2 An Approximation of the Rough Heston Model

As can be seen from the previous section, attempting to find the rHeston CF is not necessarily a trivial task since it requires the fractional Riccati ODE (3.9) to be solved. However, it is shown in El Euch *et al.* (2019) that the implementation of the rHeston CF can be greatly simplified by deriving an approximation that avoids solving fractional Riccati ODEs entirely. This is done by first simplifying the rHeston dynamics in terms of the forward variance. Then, using these simplified

dynamics, a scaled volatility of volatility parameter $\hat{\sigma}(T)$ implying rough dynamics for the cHeston CF can be determined. The approximate rough dynamics can hence be found by using the $\hat{\sigma}(T)$ parameter in the cHeston CF, implying that the tractability of the cHeston can be utilised. The derivation of this approximation is now discussed in greater detail.

3.2.1 Simplifying Rough Heston

To begin, it is shown in El Euch and Rosenbaum (2018) that the rHeston model (3.7) dynamics can be generalised by conditioning on $\mathcal{F}_t$. The main difference for the generalised rHeston dynamics is that the constant mean-reversion parameter θ in (3.7) is replaced by an $\mathcal{F}_t$-measurable function $\theta_t(u)$ to ensure the model is time consistent. Intuitively, this is since the mean-reversion of volatility now must be able to accomodate all possible terms to maturity; and so the mean-reversion parameter requires extra freedom to compensate for changes through time. Of course, the dynamics (3.7) are obtained if the mean-reversion function is made a constant for all possible time horizons. Given that the $\theta_t(u)$ is generalised to any time horizon, the integrals now reflect this also and thus will range over the time interval considered; for instance, $[t, T]$ where $t \in [0, T)$.

The addition of this mean-reversion function imposes a lot more flexibility in the rHeston model. For instance, it is shown in El Euch and Rosenbaum (2018) that the mean-reversion function can be chosen so that it is consistent with the market forward variance curve, where the forward variance is defined as $\xi_t(u) = \mathbb{E}[V_u|\mathcal{F}_t]$. This means that $\theta_t(u)$ can be written as a function of the forward variance curve and can be calibrated to the market data using variance swaps. The function relating $\theta_t(u)$ and the forward variance curve is

$$\gamma\theta_t(s) = D^\alpha\big(\mathbb{E}[V_\cdot|\mathcal{F}_t] - V_t\big)(s) + \gamma\mathbb{E}[V_s|\mathcal{F}_t], \tag{3.22}$$

where γ is the rate of mean reversion. This relationship is a consequence of solving $I^{1-\alpha}\mathbb{E}[V_t]$ which will not be derived here, but can be found in Section 3.4 of El Euch and Rosenbaum (2018). Equation (3.22) can then be substituted into the volatility dynamics of the rHeston model (3.7) to give

$$V_u = V_t + \frac{1}{\Gamma(\alpha)}\int_t^u (u-s)^{\alpha-1}\big[D^\alpha\big(\mathbb{E}[V_\cdot|\mathcal{F}_t] - V_t\big)(s) + \gamma\big(\mathbb{E}[V_s|\mathcal{F}_t] - V_s\big)\big]\, ds + [...],$$

where $[...]$ represents the remaining terms from dynamics (3.7). If it were the case that the rate of mean reversion parameter $\gamma \to 0$, then this equation could be simplified even further. This simplification is in fact motivated in Gatheral *et al.* (2018) where it is shown that there is no need for mean reversion dynamics when

$\alpha \in (\frac{1}{2}, 1)$ and is equivalent to assuming that the rate of mean reversion $\gamma \to 0$. This is plausible since Gatheral *et al.* (2018) show that $\gamma \ll 1/T$ under rough dynamics. The terms to maturity of practical interest may perhaps be 1 week at the least, but this can of course vary. By implication, choosing $\gamma = 0$ as an asymptotic result is not unrealistic given that it will always satisfy the criterion $\gamma \ll 1/T$, even if $1/T$ is quite large. Additionally, this corroborates the dynamics observed in market implied volatility, since volatility smiles flatten very quickly as the term to maturity increases. If one is to posit mean reversion, then it would imply that the mean reversion suddenly disappears as the term to maturity increases. It seems more likely that the sudden flattening of the volatility smile is some endogenous factor which fBM attempts to model. Using this simplification, the following dynamics for rHeston in terms of forward variance can be obtained:

Definition 3.4. (Simplified Rough Heston Model) A stochastic volatility process with dynamics

$$\begin{aligned} dS_t &= S_t \sqrt{V_t} dW_t \\ V_t &= \xi_u(t) + \frac{\sigma}{\Gamma(\alpha)} \int_u^t (t-s)^{\alpha-1} \sqrt{V_s} dB_s \qquad t \geq u \end{aligned} \tag{3.23}$$

is called Simplified Rough Heston (srHeston), where the forward variance is defined $\xi_u(t) = \mathbb{E}[V_t | \mathcal{F}_u]$, $\sigma > 0$, W_t and B_t are correlated BMs with $d[W, B]_t = \rho \, dt$ and $\alpha \in (\frac{1}{2}, 1)$.

This result's power lies in its simplification of the initial rHeston dynamics so that the srHeston requires only three parameters to be calibrated; that is, σ, ρ and α. Furthermore, the CF corresponding to these simplified dynamics can be derived, and is shown in El Euch and Rosenbaum (2018) to be as follows:

Theorem 3.5. ***(Simplified Rough Heston Characteristic Function)*** *Consider the srHeston model (3.23). For $t \geq 0$ and a fixed $a \in \mathbb{R}$, the characteristic function of the log stock price at some time t with terminal time T has the form*

$$\phi_t(a, T) = \exp\left(ia \log S_t + \int_t^T D^\alpha h(a, T-u) \xi_t(u) du \right), \tag{3.24}$$

where $h(a, \cdot)$ is the solution of the fractional Riccati equation

$$D^\alpha h(a,t) = \tfrac{1}{2}(-a^2 - ia) + ia\rho\sigma h(a,t) + \tfrac{1}{2}\sigma^2 h^2(a,t), \quad I^{1-\alpha} h(a,0) = 0, \tag{3.25}$$

with initial condition $h(a, 0) = 0$, which admits a unique continuous solution .

Note that CF (3.24) is written with respect to the term to maturity starting at some arbitrary time t because it is generalised with respect to $\mathcal{F}_t$. Of course, the CF defined in (3.8) can be obtained by letting $t = 0$. Further comparison of the srHeston CF (3.24) against the rHeston CF (3.8) shows that they do look very similar, except that the $I^1 h(a,t)$ term is not present in CF (3.24) since $\gamma \to 0$ in this case. The forward variance $\xi_t(u)$ term in CF (3.24) acts like the V_0 term seen in CF (3.8). For instance, if the forward variance curve were assumed to be flat so that $\xi_t(u) = V_0,\ u \in [t,T]$, then the integral part of (3.24) becomes $V_0 I^{1-\alpha} h(a,t)$, which is exactly that in CF (3.8). For fractional Riccati ODEs (3.9) and (3.25), the main difference results from their $h(a,t)$ terms since (3.25) uses the asymptotic value $\gamma \to 0$ which results in dependence upon only three parameters σ, ρ and α. It is important to note that for the srHeston that σ has no dependence on the value of γ as from Theorem 3.3 which is why $\gamma \to 0$ does not imply $\sigma \to 0$ for the srHeston.

To find a suitable solution $h(a,t)$ for fractional Riccati ODE (3.25), the numerical methods as described in Section 3.1.3 can be implemented since there is no fundamental change in the structure of this newly derived fractional Riccati ODE. The goal, however, is to find another way to approximate the rHeston without solving a fractional ODE. This is done by finding a scaled volatility of volatility parameter that derives rough dynamics, and is the genesis of the Poor Man's Heston (pmHeston) approximation.

3.2.2 The Poor Man's Heston Approximation

To find the scaled volatility of volatility parameter, it is required that the realised variance is computed (El Euch and Rosenbaum, 2018). The realised variance is the total variance that occurs over some specified time horizon, and in this case is defined as $\int_t^T V_u du$; i.e., the sum of the variance at each time point. Then, by taking the square-root of the variance of the realised variance, the volatility of volatility parameter could be found as desired. Now, supposing that $t = 0$ so that the time horizon for some terminal time T is $[0,T]$, the realised variance dynamics implied from dynamics (3.23) for the srHeston are found as follows:

$$\begin{aligned}
\int_0^T V_u du &= \int_0^T \xi_0(u) du + \int_0^T \int_0^u \frac{\sigma}{\Gamma(\alpha)} (u-s)^{\alpha-1} \sqrt{V_s}\, dB_s\, du \\
&= \int_0^T \xi_0(u) du + \int_0^T \int_s^T \frac{\sigma}{\Gamma(\alpha)} (u-s)^{\alpha-1} \sqrt{V_s}\, du\, dB_s \\
&= \int_0^T \xi_0(u) du + \int_0^T \frac{\sigma}{\Gamma(\alpha)} \left[\int_s^T (u-s)^{\alpha-1}\, du \right] \sqrt{V_s}\, dB_s.
\end{aligned}$$

Noting that $\int_s^T (u-s)^{\alpha-1}\, du = \frac{1}{\alpha}(T-s)^{\alpha}$, and changing the dummy variable s with u where necessary, the following is obtained for the realised variance:

$$\int_0^T V_u du = \int_0^T \xi_0(u) du + \frac{\sigma}{\Gamma(\alpha+1)} \int_0^T (T-u)^{\alpha} \sqrt{V_u}\, dB_u, \tag{3.26}$$

by using the fact that $\alpha\Gamma(\alpha) = \Gamma(\alpha+1)$. What remains is to find the variance of the realised variance. To do this, note that the stochastic integral is with respect to Brownian Motion, a martingale, and the integrand is a predictable function. Therefore, the stochastic integral is itself a martingale implying it has zero mean. The realised variance hence has an expectation equal to the first integral of equation (3.26). Then, the Itô Isometry $\mathbb{E}\big[(\int_0^T H_s dM_s)^2\big] = \mathbb{E}\big[\int_0^T H_s^2 d[M]_s\big]$, where H_s is a predictable process, and dM_s is a martingale integrator, can be applied to calculate the variance. It follows that

$$\begin{aligned}
\text{Var}\left(\int_0^T V_u du\right) &= \mathbb{E}\left[\left(\int_0^T V_u du - \mathbb{E}\left(\int_0^T V_u du\right)\right)^2\right] \\
&= \mathbb{E}\left[\left(\int_0^T \frac{\sigma(T-u)^{\alpha}}{\Gamma(\alpha+1)} \sqrt{V_u}\, dB_u\right)^2\right] \\
&= \int_0^T \frac{\sigma^2 (T-u)^{2\alpha}}{\Gamma(\alpha+1)^2} \xi_0(u) du
\end{aligned}$$

since $\mathbb{E}[V_u] = \xi_0(u)$. Using this result, it is shown in El Euch and Rosenbaum (2018) that to find the scaling factor involves equating this to the classical Heston case, when $\alpha = 1 \iff H = \frac{1}{2}$. By equating these cases, the volatility of volatility parameter $\hat{\sigma}(T)$ for the term to maturity T implied in the cHeston can be found as follows:

$$\int_0^T \frac{\sigma^2 (T-u)^{2\alpha}}{\Gamma(\alpha+1)^2} \xi_0(u) du = \hat{\sigma}(T)^2 \int_0^T (T-u)^2 \xi_0(u) du,$$

so that the scaled volatility of volatility $\hat{\sigma}(T)$ has the form

$$\hat{\sigma}(T) = \frac{\sigma}{\Gamma(\alpha+1)} \sqrt{\frac{\int_0^T (T-u)^{2\alpha} \xi_0(u) du}{\int_0^T (T-u)^2 \xi_0(u) du}}. \tag{3.27}$$

Since this is now the volatility of volatility parameter expected to be found in the cHeston case, it is possible to derive a cHeston CF in a similar way as was done in Section 3.1.1. However, since the forward variance curve $\xi_0(u)$ would have to be used instead of a constant variance V_u in the "guessed" form of the CF as in equation (3.3), solving for the CF would be challenging. Instead, a more eloquent way of finding the implied cHeston CF involves using the results of Theorem 3.5. By using $\alpha = 1$ and the implied volatility of volatility parameter $\hat{\sigma}(T)$, the parameters

that yields the cHeston CF is obtained. The implied cHeston CF is of the form:

$$\phi_t(a,T) = \exp\left(ia\log S_t + \int_t^T \partial_u h(a,T-u)\xi_t(u)du\right),$$

with a classical Riccati ODE of the form:

$$\partial_u h(a,t) = \tfrac{1}{2}(-a^2 - ia) + ia\rho\hat{\sigma}(T)h(a,t) + \tfrac{1}{2}\hat{\sigma}(T)^2 h^2(a,t), \quad h(a,0) = 0.$$

Then, using techniques to solve the Riccati ODE as seen in Section 3.1.1, the classical Heston CF with scaled volatility of volatility parameter can be obtained. This implies that rHeston for some term to maturity can be approximated by using the cHeston CF as seen in Appendix A.3 with the only difference that $\hat{\sigma}(T)$ is substituted in place of the original volatility of volatility parameter σ.

The last simplification to determine the pmHeston approximation requires the assumption that the forward variance curve is flat; i.e., to assume that $\xi_0(u) = V_0,\ u \in [0,T]$, where V_0 is the initial variance. Using this assumption, it can be seen that the scaled volatility of volatility simplifies to:

$$\begin{aligned}\hat{\sigma}(T) &= \frac{\sigma}{\Gamma(\alpha+1)}\sqrt{\frac{\int_0^T (T-u)^{2\alpha}du}{\int_0^T (T-u)^2 du}} \\ \Rightarrow \hat{\sigma}(T) &= \frac{\sigma T^{\alpha-1}}{\Gamma(\alpha+1)}\sqrt{\frac{3}{2\alpha+1}}.\end{aligned} \tag{3.28}$$

Chapter 4

Methodology and Implementation

4.1 Pricing Under Rough Volatility

By using the fractional Adam's Method in Section 3.1.3 to solve fractional Riccati ODEs, an implementation using the CF of the rHeston model for pricing can be demonstrated. Using Fourier techniques and the rHeston CF, the probability that an option is exercised can be determined which, in turn, means that options can be priced. This is done by using the well-known Inversion Theorem of Gil-Pelaez (1951). It is stated as follows:

Theorem 4.1. ***(Gil-Pelaez Inversion Theorem)*** *Given a characteristic function ϕ_X associated with a random variable $X : \Omega \to \mathbb{R}$, for $k \in \mathbb{R}$*

$$\mathbb{P}\{X > k\} = \frac{1}{2} + \frac{1}{\pi}\int_0^\infty Re\left[\frac{e^{-iuk}\phi_X(u)}{iu}\right] du.$$

If a call option is considered, it is simple to derive a general option pricing formula (shown in Appendix A.5) which takes on the form:

$$C_t(K) = S_0 P_1 - K \exp\left(-\int_0^t r_u du\right) P_2, \tag{4.1}$$

where P_1 and P_2 are probabilities of exercise under different equivalent martingale measures (EMMs) for a call option denoted $C_t(K)$ with maturity T priced at time t, a strike price K, and a short rate r_t. This is done by using *change of numéraire invariance*, an incredibly convenient technique developed in Geman *et al.* (1995). Then, by using a discretization scheme of the Gil-Pelaez Theorem similar to that in Joshi (2011), the probabilities of exercise for a call option can be determined to be

$$P_1 = \mathbb{Q}^s\{s > k\} = \frac{1}{2} + \frac{1}{\pi}\sum_{n=1}^{N} \text{Re}\left[\frac{e^{-iu_n k}\phi(u_n - i)}{iu_n\phi(-i)}\right]\Delta u, \tag{4.2}$$

$$P_2 = \mathbb{Q}\{s > k\} = \frac{1}{2} + \frac{1}{\pi}\sum_{n=1}^{N} \text{Re}\left[\frac{e^{-iu_n k}\phi(u_n)}{iu_n}\right]\Delta u, \tag{4.3}$$

where s and k are the log stock and strike price, respectively, $\mathbb{Q}_s$ is the EMM with s as the numéraire, and $\mathbb{Q}$ is the risk-neutral measure. The integration limits are restricted to $[0, u_{\max}]$, and hence the discrete grid is $u_n = (n - \frac{1}{2})\Delta u$, where $\Delta u = u_{\max}/N$.

Using the results of Theorem 3.3 and the Gil-Pelaez Inversion Theorem, it is possible to test the accuracy of option prices generated. This is done by using $\alpha = 1$ so this method can be compared to the option prices generated from the closed-form CF of the cHeston in Section 3.1.1 (also displayed in Appendix A.3). Using these pricing techniques, the outputs displayed in Table 4.1 are produced.

Altered Parameters	Closed-Form Heston	Rough Heston	Error
None	9.7511891	9.7519466	7.5747553e-04
$\rho = 0.2$	9.7106106	9.7115443	9.3373710e-04
$\gamma = 2$	18.4361064	18.4374343	1.3279387e-03
$V_0 = 0.06$	11.2690010	11.2699065	9.0553376e-04

Tab. 4.1: Rough Heston ($\alpha = 1$) vs Closed-Form Heston ATM Call Option Prices (Rounded to 7 Decimal Places) for Parameter Values $\gamma = 0.1$, $\rho = -0.671$, $V_0 = 0.0392$, $\sigma = 0.4061$, $\nu = \sigma/\gamma$, $\theta = 0.3156$, $r = 0.03$, $S_0 = K = 100$, and $T = 1$.

The first row of Table 4.1 shows the price obtained by using the parameters that are displayed in its caption, whereas the other three rows show the prices produced when changing only the parameter shown in the first column. Given an appropriate mesh size, it can be seen that the prices generated with the rHeston CF are quite accurate. For all intents and purposes, it can be concluded that the rHeston is suitable for pricing European options.

4.2 Implied Volatility Surfaces and ATM Skews

Using the methods to price European options as in Section 4.1, it is then simple to find the Black-Scholes implied volatility. In this case, the MATLAB function *blsimpv(·)* is used, but this can also be done by using a standard objective function and an in-built numerical solver. The log-moneyness is defined as $\log(K/S)$, and the α is chosen to be close to that of the Hurst parameter for the S&P Index in Gatheral *et al.* (2018) to allow for the comparison of results. Of course, using log-moneyness $= \log(S/K)$ achieves the same outcome, but with inverted axes. Implementation of these methods results in the IV surface displayed in Figure 4.1.

It can be seen that this rHeston IV surface is very similar to the actual IV of the S&P Index in Gatheral *et al.* (2018) on page 2. Figure 4.1 shows the increased

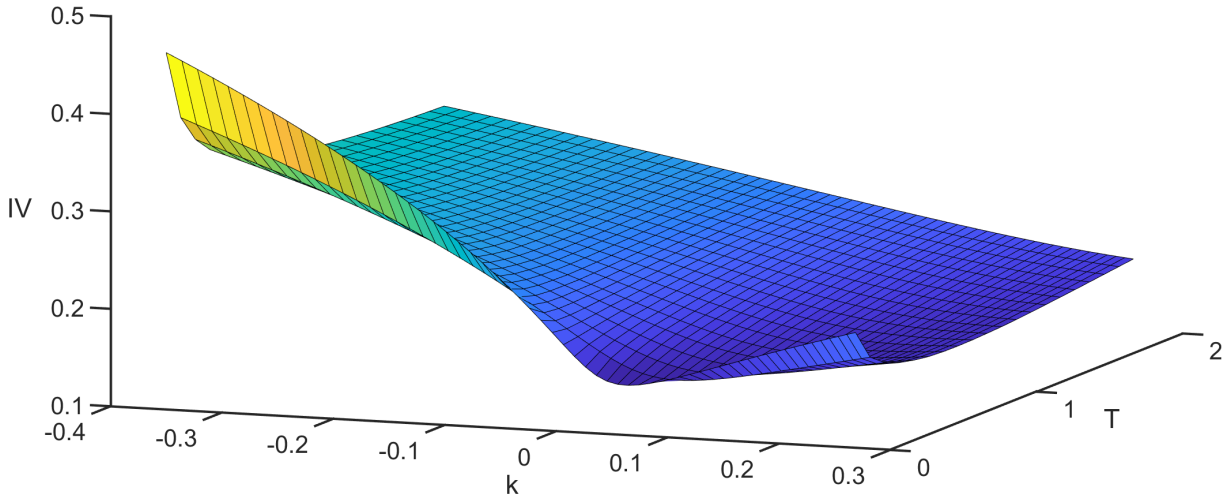

Fig. 4.1: Implied volatility surface from Rough Heston prices using a short rate of $r = 0.03$, with parameters $\alpha = 0.6474$, $\gamma = 0.1$, $\rho = -0.671$, $V_0 = 0.0392$, $\sigma = 0.4061$ and $\theta = 0.3156$.

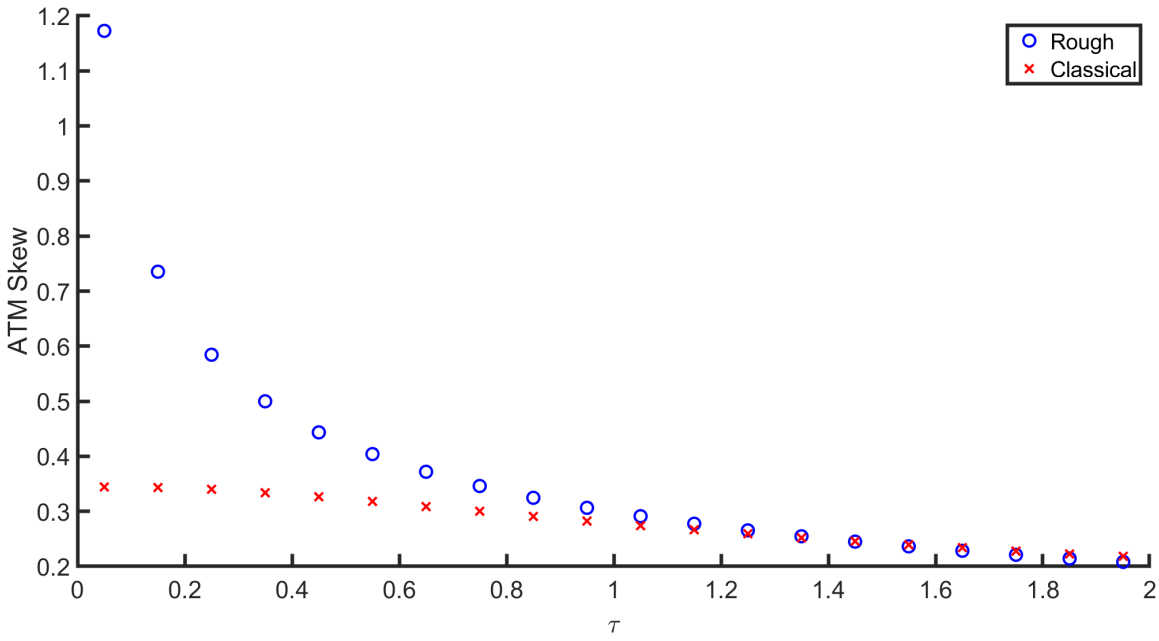

Fig. 4.2: Rough Heston vs Classical Heston TS ATM Skew using parameters as in Figure 4.1.

volatility of options with shorter maturities and for those that are OTM and ITM, as was desired. Furthermore, the volatility decreases quickly with an increasing term to maturity which confirms the feasibility of the assumption made in Gatheral *et al.* (2018) that the rate of mean reversion parameter $\gamma \to 0$. Once again, it is

emphasized that a suitably large $u_{\max}$ and N are chosen so that the option prices and consequently the IV values converge appropriately (Appendix B.4).

Even though the IV surface appears to be realistic, it is important to consider the TS ATM skew, defined $\psi(\tau) := \left|\frac{\partial}{\partial k}\sigma_{BS}(k,\tau)\right|_{k=0}$ as seen in Chapter 2. This is an important indicator as it allows one to more accurately compare the implied volatilities produced by different models (Bayer *et al.*, 2016). It is desired that the rHeston model captures an explosion in the rate of change of IV as the term to maturity shortens so that a plot similar to that of the S&P Index in Figure 2.1 is attained. This behaviour is corroborated by the power-law shape seen in Figure 4.2, and is comparable to the TS ATM skew seen in Figure 2.1. Comparison to the TS ATM skew of the cHeston shows that it is insufficient at capturing this explosive nature at shorter terms to maturity.

4.3 Poor Man's Heston

The viability of the pmHeston approximation is tested against an IV surface generated using the srHeston dynamics. In practice, the srHeston parameters would be calibrated to the market IV data, however, it is assumed that the arbitrary parameters chosen here are sufficient for the purposes of testing the approximation. Using MATLAB and the methods in Sections 4.1 and 4.2, the IV surfaces displayed in Figure 4.3 are produced.

Initial appraisal confirms that the pmHeston approximation is good given that it captures the smile dynamics as desired despite the simplification in it's CF (Figure 4.3). Note, however, that the % Error Plot shows that the pmHeston approximation loses accuracy as the term to maturity shortens. Given that % error for terms to maturity of less than 0.5 years encompasses about 30% of the total error, it can be argued that the pmHeston is an insufficient approximation of the srHeston. However, to further assess the quality of the approximation, the smiles for different terms to maturity of the srHeston and pmHeston are compared in Figure 4.4 as is done in El Euch *et al.* (2019). These plots corroborate the efficacy of the pmHeston approximation at capturing the smile dynamics over different terms to maturity. Despite the % errors at shorter terms to maturity, the pmHeston approximation is still very impressive given that it is so east to implement. Notice that as T increases, the smiles become flatter as expected, but the hockey-stick shape of the smiles remain. This shows consistency of the pmHeston approximation over different terms to maturity, and is attributed to the appropriate scaling of the volatility of volatility parameter.

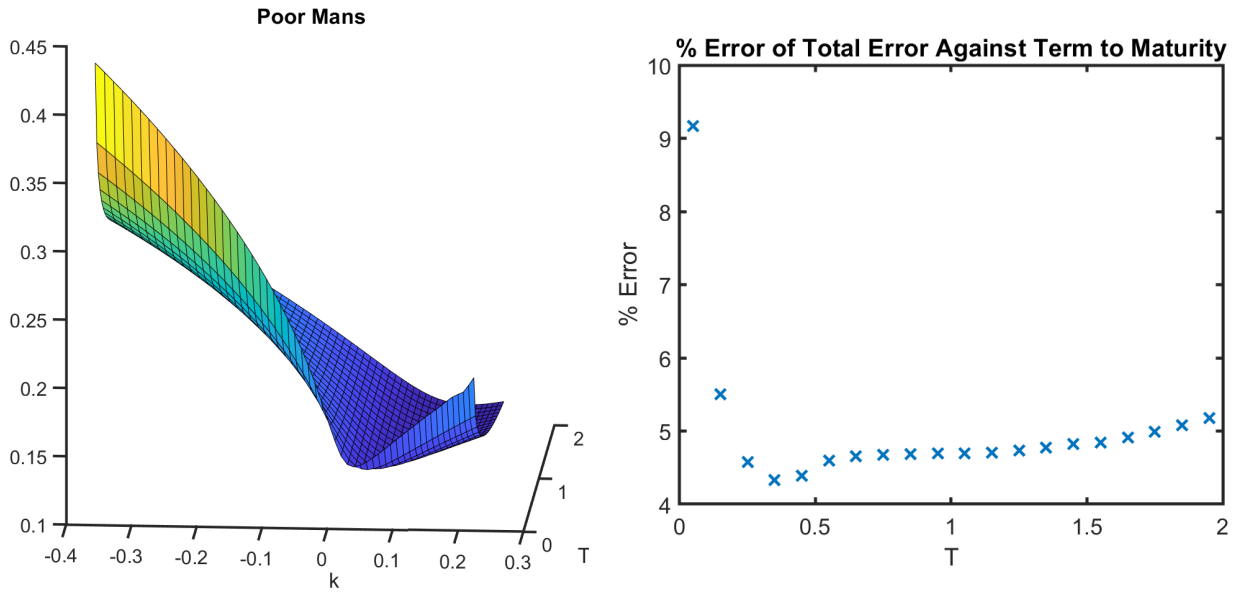

Fig. 4.3: Poor Man's Heston IV surface and corresponding % Error Plot using the Simplified Rough Heston as a baseline. The parameters used are $r = 0.03$, $\xi_0(u) = 0.0392\ \forall u \in [0, T]$, $\alpha = 0.5474$, $\rho = -0.671$ and $\sigma = 0.4061$.

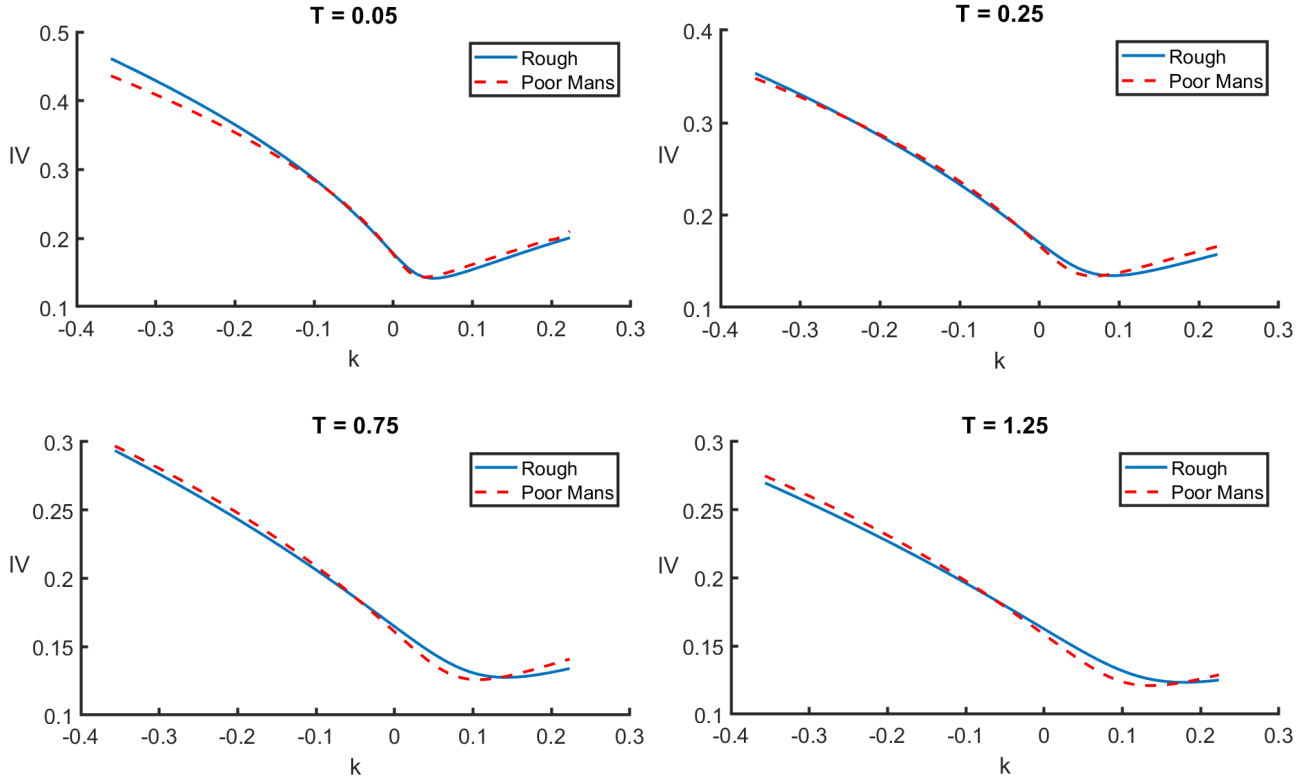

Fig. 4.4: Rough Heston vs Poor Man Heston smiles for different terms to maturity for the same parameters as in Figure 4.3.

Furthermore, analysis of the TS ATM IV skew of the pmHeston shows that it has the power-law shape that is desired to infer rough dynamics (Figure 4.5). It is expected that the pmHeston will have larger TS ATM IV skew values given the more convex features that it has relative to the srHeston, as noticed in the Figure 4.4. Using these results, it can hence be concluded that the pmHeston sufficiently approximates rough volatility dynamics.

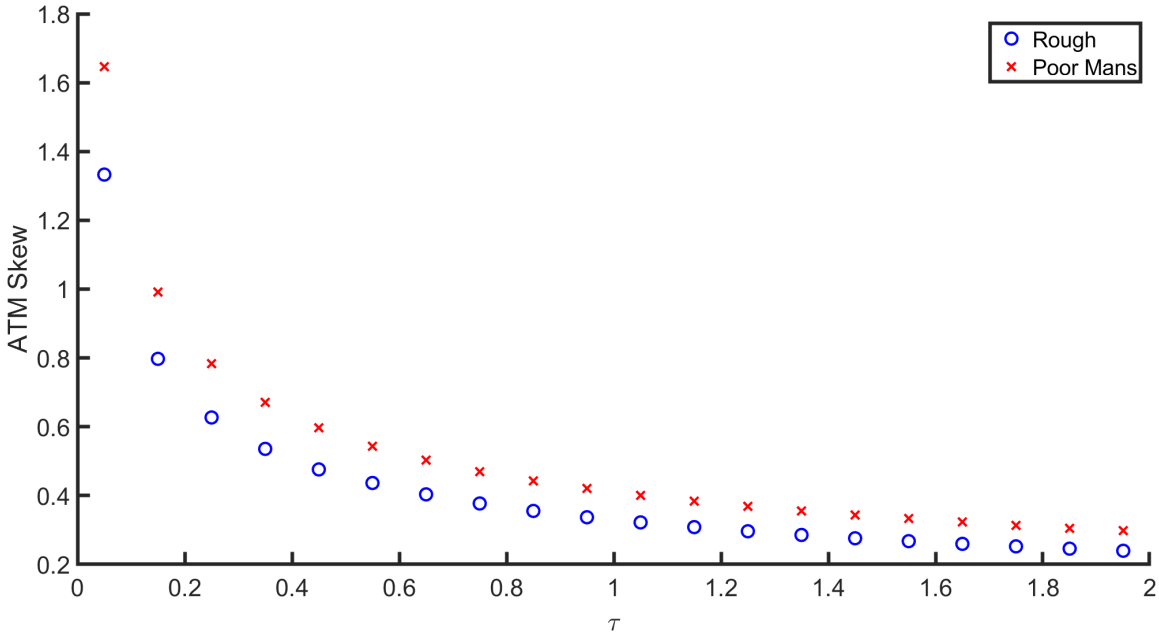

Fig. 4.5: Rough Heston vs Poor Man Heston TS ATM IV skew for the same parameters as in Figure 4.3.

Chapter 5

Conclusion

Literature such as Gatheral *et al.* (2018), Fukasawa (2011) and Rosenbaum (2011) was explored, and it was concluded that the volatility implied from market data has rough dynamics. It was discovered that rough dynamics imply the usage of fractional Brownian Motion, as defined in Mandelbrot and Van Ness (1968), which was characterised by its power-law kernel and Hurst parameter. Importantly, the Hurst parameter implied from volatility data was found to be $H \in (0, \frac{1}{2})$ which contrasts the stylised notion of long-memory in volatility processes postulated in older literature. This finding was concluded from the studies of the TS ATM skew of the S&P Index as in Gatheral *et al.* (2018), and also from using the microstructure noise index measure as presented in Rosenbaum (2011).

Given the supporting evidence for the rough dynamics of market volatility, models using these dynamics were then considered. The rough Heston (rHeston), a generalisation of the classical Heston (cHeston), was the model of choice given its ubiquity in the literature. To create the necessary foundation for understanding the rHeston, the cHeston was first studied and its characteristic function (CF) was derived using techniques from Heston (1993) and El Euch and Rosenbaum (2019). The derivation of the rHeston model from El Euch and Rosenbaum (2019) was then discussed, and it could be concluded by comparing these models that the rHeston was indeed a generalistion of the cHeston. This was further reinforced from the essential Theorem 3.3 derived in El Euch and Rosenbaum (2019) which showed that the structure of the cHeston and rHeston CFs as well as their associated Riccati ODEs were indeed very similar.

It was determined that the most distinctive feature of the rHeston CF was its fractional Riccati ODE which required numerical methods to solve. Three methods were considered and derived, with the most accurate being the Fractional Adam's Method from Diethelm *et al.* (2002). It was discovered that this method was in fact the fractional equivalent of the Adams-Bashforth-Moulton algorithm, and involved using a predictor to correct for any bias in approximation. The necessity of the pre-

dictor was discussed, and it was concluded that it was requisite for pricing options under rough dynamics as it enabled more accurate approximations for larger terms to maturity. Additionally, this method was seen to be incredibly useful for solving fractional ODEs in general, given its high accuracy and efficiency.

Given the complexity that the fractional Riccati ODE adds to the rHeston model, simplifications and approximations of the rHeston CF were considered. The first approach taken was to simplify the rHeston CF by using the forward variance curve, defined $\xi_t(s) = \mathbb{E}[V_s|\mathcal{F}_t]$, as shown in El Euch *et al.* (2019). To start, a generalisation of the rHeston CF conditioned on $\mathcal{F}_t$ was found. This resulted in the mean reversion parameter θ generalising to $\theta_t(s)$, an $\mathcal{F}_t$-measurable function for the specified time horizon. In addition, the relationship $\gamma\theta_t(s) = D^\alpha\big(\mathbb{E}[V_\bullet|\mathcal{F}_t] - V_t\big)(s) + \gamma\mathbb{E}[V_s|\mathcal{F}_t]$ from El Euch and Rosenbaum (2018) was needed to link the mean-reversion parameter $\theta_t(s)$ to the forward variance curve $\xi_t(s)$. Using this result, the simplified rough Heston (srHeston) dynamics could then be inferred by assuming that the rate of mean reversion parameter γ tended to 0. This assumption was motivated by the findings in Gatheral *et al.* (2018) in which it was concluded that $\gamma \ll 1/T$ under rough dynamics. Manipulating the rHeston CF using these simplifcations resulted in the srHeston CF seen in Theorem 3.5.

To remove the complexity arising from the fractional Riccati ODEs in the srHeston altogether, the derivation of the Poor Man's Heston (pmHeston) approximation from El Euch *et al.* (2019) was studied. This derivation involved linking the cHeston and the srHeston so that the simpler cHeston CF with an adjusted volatility parameter for each term to maturity could be used. This volatility parameter was calculated by determining the variance of the realised variance of the srHeston, and then equating it to the implied cHeston case for $\alpha = 1$. From there, the scaled volatility of volatility could be solved to yield a value:

$$\hat{\sigma}(T) = \frac{\sigma}{\Gamma(\alpha+1)}\sqrt{\frac{\int_0^T (T-u)^{2\alpha}\xi_0(u)du}{\int_0^T (T-u)^2\xi_0(u)du}}.$$

To achieve the pmHeston approximation, the forward variance curve was assumed to be flat; i.e. $\xi_0(u) = V_0\ \forall u \in [0,T]$. Under this assumption, the scaled volatility of volatility parameter was concluded to be

$$\hat{\sigma}(T) = \frac{\sigma T^{\alpha-1}}{\Gamma(\alpha+1)}\sqrt{\frac{3}{2\alpha+1}}.$$

By using these various Theorems and results, it was possible to solve the fractional Riccati ODEs and to implement the pricing of options using the Inversion Theorem of Gil-Pelaez (1951). Volatility surfaces were then plotted by finding the Black-

Scholes implied volatilities from the simulated prices. The volatility surfaces obtained were accurate and realistic, and it was concluded that these models were suitable for capturing the rough dynamics of market volatility. Lastly, it was observed that the pmHeston provided a very good approximation of rough volatility dynamics, and was the most tractable method for modelling rough volatility dynamics.

Bibliography

Bayer, C., Friz, P. and Gatheral, J. (2016). Pricing Under Rough Volatility, *Quantitative Finance* **16**(6): 887–904.

Diethelm, K., Ford, N. J. and Freed, A. D. (2002). A Predictor-Corrector Approach for the Numerical Solution of Fractional Differential Equations, *Nonlinear Dynamics* **29**(1-4): 3–22.

Diethelm, K. and Freed, A. D. (1998). The FracPECE Subroutine for the Numerical Solution of Differential Equations of Fractional Order, *Forschung und wissenschaftliches Rechnen* **1999**: 57–71.

Dupire, B. (1994). Pricing with a Smile, *Risk* **7**(1): 18–20.

Egorov, A. I. (2007). *Riccati Equations*, Pensoft Publishers.

El Euch, O., Gatheral, J. and Rosenbaum, M. (2019). Roughening Heston, *Risk* pp. 84–89.

El Euch, O. and Rosenbaum, M. (2018). Perfect Hedging in Rough Heston Models, *Annals of Applied Probability* **28**(6): 3813–3856.

El Euch, O. and Rosenbaum, M. (2019). The Characteristic Function of Rough Heston Models, *Mathematical Finance* **29**(1): 3–38.

Fouque, J.-P., Papanicolaou, G., Sircar, R. and Solna, K. (2004). Maturity Cycles in Implied Volatility, *Finance and Stochastics* **8**(4): 451–477.

Fukasawa, M. (2011). Asymptotic Analysis for Stochastic Volatility: Martingale Expansion, *Finance and Stochastics* **15**(4): 635–654.

Gatheral, J., Jaisson, T. and Rosenbaum, M. (2018). Volatility is Rough, *Quantitative Finance* **18**(6): 933–949.

Geman, H., El Karoui, N. and Rochet, J.-C. (1995). Changes of Numeraire, Changes of Probability Measure and Option Pricing, *Journal of Applied probability* pp. 443–458.

Gil-Pelaez, J. (1951). Note on the Inversion Theorem, *Biometrika* **38**(3-4): 481–482.

Heston, S. L. (1993). A Closed-Form Solution for Options with Stochastic Volatility with Applications to Bond and Currency Options, *The Review of Financial Studies* **6**(2): 327–343.

Hunt, P. and Kennedy, J. (2004). *Financial Derivatives in Theory and Practice*, John Wiley & Sons.

Joshi, M. S. (2011). *More Mathematical Finance*, Pilot Whale Press.

Kythe, P. and Puri, P. (2011). *Computational Methods for Linear Integral Equations*, Springer Science & Business Media.

Mandelbrot, B. B. and Van Ness, J. W. (1968). Fractional Brownian Motions, Fractional Noises and Applications, *SIAM review* **10**(4): 422–437.

Miller, D. A. (2004). Fractional Calculus, *Minor Thesis part of PHD* .

Nourdin, I. (2012). *Selected Aspects of Fractional Brownian Motion*, Vol. 4, Springer.

Rogers, L. C. G. (1997). Arbitrage with Fractional Brownian Motion, *Mathematical Finance* **7**(1): 95–105.

Rosenbaum, M. (2009). First Order P-Variations and Besov Spaces, *Statistics & Probability Letters* **79**(1): 55–62.

Rosenbaum, M. (2011). A New Microstructure Noise Index, *Quantitative Finance* **11**(6): 883–899.

Shevchenko, G. (2014). Fractional Brownian Motion in a Nutshell, *Preprint arXiv: 1406.1956* .

Appendix A

Ancillary Results and Derivations

A.1 Fractional Calculus

Fractional calculus is a generalisation of canonical calculus in the sense that for differentiation and integration, the operation is performed to the α^{th} order, for $\alpha > 0$. This of course includes α values that are not integers and are hence "fractional". The subsequent results follow from the work presented in Miller (2004)

Beginning with fractional integration as a generalisation, it was originally noticed by Cauchy that a repeated formula for integration existed, and is given as

$$I^n f(x) = \frac{1}{(n-1)!} \int_0^x (x-t)^{n-1} f(t) dt$$

Given that the gamma function $\Gamma(z) = \int_0^\infty t^{z-1} e^{-t} dt$ has the property that $\Gamma(z+1) = z\Gamma(z)$ which can be shown using integration by parts, it follows that for $n \in \mathbb{N}$ that $\Gamma(n+1) = n!$ by recursion. Hence, the Cauchy repeated integration formula for $\alpha \in \mathbb{R}^+$ can be written as:

$$I^\alpha f(x) = \frac{1}{\Gamma(\alpha)} \int_0^x (x-t)^{\alpha-1} f(t) dt \tag{A.1}$$

where (A.1) is in fact the definition of a fractional integral. In a similar vain, the fractional derivative is defined as

$$D^\alpha f(x) = \frac{1}{\Gamma(\alpha-1)} \frac{d}{dt} \int_0^x (x-t)^{-\alpha} f(t) dt \tag{A.2}$$

A.2 Solving Riccati ODEs

For a non-linear Riccati ODE of the form

$$y'(t) = a(t)y^2(t) + b(t)y(t) + c(t) \tag{$*$}$$

consider the linear ODE

$$\omega''(t) - \left(\frac{a'(t)}{a(t)} + b(t) \right) \omega'(t) + a(t)c(t)\omega = 0 \tag{$\dagger$}$$

It can be shown that if $\omega(t)$ is the general solution of the 2$^{\text{nd}}$ order homogenous linear ODE $(\dagger)$, then the solution of $(*)$ is

$$y(t) = -\frac{\omega'(t)}{\omega(t)a(t)} \tag{A.3}$$

This can be easily shown: For the sake of solving the classical Heston Riccati ODE, assume that a, b and c are constant. Then to obtain the general solution of $(\dagger)$, choose $\omega = e^{xt}$. Substitute this into $(\dagger)$ to get

$$e^{xt}(x^2 - bx + ac) = 0$$

Then both roots of the auxiliary polynomial part x_+ and x_- are solutions. By the principle of superposition, the sum of both solutions multiplied by some scalar factor is the general solution; i.e. $\omega = C_1 e^{x_+ t} + C_2 e^{x_- t}$. "Guessing" solution A.3, this is substituted into $(*)$ to get:

$$\begin{aligned}
-\frac{\omega''}{a\omega} + \frac{a(\omega')^2}{a^2\omega^2} &= a\frac{(\omega')^2}{a^2\omega^2} - b\frac{\omega'}{a\omega} + c \\
-\omega''a\omega + a(\omega')^2 &= a(\omega')^2 - ab\omega'\omega + a^2c\omega^2 \\
0 &= \omega''a\omega - ab\omega'\omega + a^2c\omega^2 \\
0 &= a\omega(\omega'' - b\omega' + ac\omega)
\end{aligned}$$

Now since ω is chosen to be a solution of $(\dagger)$, we must have that $\omega'' - b\omega' + ac\omega = 0$ also. And hence, the general solution for $y(t)$ is consistent. This derivation is inspired from work presented in Egorov (2007).

A.3 Classical Heston Characteristic Function

The characteristic function of the log-stock price is given by:

$$\phi(u) = \exp(g + hV_0 + ia\log(S_0)) \tag{A.4}$$

where

$$\begin{aligned}
h &= \frac{(1 - e^{-Tm})x^-}{1 - ne^{-Tm}} \\
g &= rTia + \theta\gamma\left(Tx^- - \frac{1}{v}\log\left\{\frac{1 - ne^{-Tm}}{1 - n}\right\}\right)
\end{aligned}$$

with $v = \frac{\sigma^2}{2}$, $b = \gamma - \rho\sigma ia$, $c = -\frac{a^2 + ia}{2}$, $m = \sqrt{b^2 - 4vc}$, $x^{\pm} = \frac{b \pm m}{2v}$, $n = \frac{x^-}{x^+}$ and $\sigma = \gamma\nu$.

A.4 Fractional Adams Method

The fractional Riccati Equation (3.9) can be defined as

$$D^{\alpha}h(a,t) = F(a, h(a,t)), \qquad I^{1-\alpha}h(a,0) = 0,$$

where

$$F(a,x) = \tfrac{1}{2}(-a^2 - ia) + \gamma(ia\rho\nu - 1)x + \tfrac{1}{2}(\gamma\nu)^2 x^2$$

To find an estimate of the solution $h(a,t)$, notated as $\hat{h}(a,t)$, the fractional Adams method can be applied as follows:

Define weights

$$\begin{aligned}
a_{0,n+1} &= \tfrac{\Delta^\alpha}{\Gamma(\alpha+2)}\big(n^{\alpha+1} - (n-\alpha)(n+1)^\alpha\big),\\
a_{j,n+1} &= \tfrac{\Delta^\alpha}{\Gamma(\alpha+2)}\big((n-j+2)^{\alpha+1} + (n-j)^{\alpha+1} - 2(n-j+1)^{\alpha+1}\big), \quad \text{for } 1 \le j \le n\\
a_{n+1,n+1} &= \tfrac{\Delta^\alpha}{\Gamma(\alpha+2)}\\
b_{j,n+1} &= \tfrac{\Delta^\alpha}{\Gamma(\alpha+1)}\big((n-j+1)^\alpha - (n-j)^\alpha\big), \quad \text{for } 0 \le j \le n
\end{aligned}$$

For some mesh Δ where time $t_j = t_0 + j\Delta$

A predictor $\hat{h}^p(a,t)$ is used since the initial formulation of the solution results in an implicit scheme, and so the predictor overcomes this issue. Hence, the final explicit scheme with the associated predictor is found by applying the following:

$$\begin{aligned}
\hat{h}^p(a,t_{n+1}) &= \sum_{0\le j\le n} b_{j,n+1} F(a,\hat{h}(a,t_j)), \qquad \hat{h}(a,0) = 0\\
\Rightarrow \hat{h}(a,t_{n+1}) &= a_{0,n+1}F(a,\hat{h}(a,0)) + a_{n+1,n+1}F(a,\hat{h}^p(a,t_{n+1}))\\
&\quad + \sum_{1\le j\le n} a_{j,n+1}F(a,\hat{h}(a,t_j))
\end{aligned}$$

The presentation of this scheme is derived from the appendix in Diethelm *et al.* (2002) and Section 5.1 in El Euch and Rosenbaum (2019), both of which can be consulted for further details.

A.5 Fourier Techniques in Option Pricing

To begin, the following definitions are stated:

Definition A.1. (Fourier Transform) Let $f : \mathbb{R} \to \mathbb{C}$ be an $\mathcal{L}^1$ integrable function. Then the *Fourier Transform* of f is defined as

$$f^*(\omega) = \int_{-\infty}^{\infty} e^{i\omega x} f(x)dx$$

If f is continuous and f^* is also $\mathcal{L}^1$ integrable, then the *Fourier Inversion Formula* is defined as

$$f(x) = \frac{1}{2\pi}\int_{-\infty}^{\infty} e^{-i\omega x} f^*(\omega)d\omega$$

Definition A.2. (Characteristic Function) If X is a random variable, then its characteristic function $\phi_X : \mathbb{R} \to \mathbb{C}$ is defined by

$$\phi_X(u) = \mathbb{E}\left[e^{iux}\right]$$

If X has probability density function (pdf) $f_X : \mathbb{R} \to \mathbb{R}$, then the characteristic function may be written as

$$\phi_X(u) = \int_{-\infty}^{\infty} e^{iux} f_X(x) dx$$

Combining these definitions, notice that the second relationship for the characteristic function implies that it is a Fourier transform of the density function. Hence, the density function can be constructed from the characteristic function using the Fourier inversion formula.

These techniques can be used to derive a general option pricing formula. In this case, a call option is considered. It is desired to change the numéraire from the bank account to the stock process S_t. Let $\mathbb{Q}$ be the risk-neutral equivalent martingale measure (EMM) with numéraire $A_t = \exp(\int_0^t r_u du)$, where r_t is the short rate, either deterministic or stochastic. Similarly, define $\mathbb{Q}^s$ to be the EMM with respect to numéraire S_t. Then for a call option with maturity T, a price at time t of, say, C_t and strike K

$$\begin{aligned} C_t(K) &= A_0 \mathbb{E}_{\mathbb{Q}} \left[\frac{(S_T - K)\mathbb{I}_{S_T > K}}{A_T} \right] \\ &= A_0 \mathbb{E}_{\mathbb{Q}} \left[\frac{S_T}{A_T} \mathbb{I}_{S_T > K} \right] - K \mathbb{E}_{\mathbb{Q}} \left[\exp\left(-\int_0^t r_u du \right) \mathbb{I}_{S_T > K} \right] \\ &= S_0 \mathbb{E}_{\mathbb{Q}^s} \left[\frac{S_T}{S_T} \mathbb{I}_{S_T > K} \right] - K \mathbb{E}_{\mathbb{Q}} \left[\exp\left(-\int_0^t r_u du \right) \mathbb{I}_{S_T > K} \right] \end{aligned}$$

where the last step is performed by change of numéraire invariance. This is equivalent to a change of measure by using a Radon-Nikodým derivative $\frac{d\mathbb{Q}^s}{d\mathbb{Q}} = \frac{S_T A_0}{S_0 A_T}$. Assuming that the short rate r_t is deterministic, the above equation simplifies to the following general option pricing pricing formula for a call:

$$C_t(K) = S_0 \mathbb{Q}^s\{S_T > K\} - K \exp\left(-\int_0^t r_u du \right) \mathbb{Q}\{S_T > K\} \tag{A.5}$$

In order to calculate these probabilities, it is required that the log-stock and -strike prices are utilised so that the characteristic function is also involved. Hence, for $s = \log S_T$ and $k = \log K$, the characteristic function under $\mathbb{Q}$ is $\phi_s(u) = \mathbb{E}_{\mathbb{Q}}[e^{ius}]$. Consequently, $\mathbb{E}_{\mathbb{Q}}[S_T] = \mathbb{E}_{\mathbb{Q}}[e^{\log S_T}] = \phi_s(-i)$. Now, noticing that $\mathbb{E}_{\mathbb{Q}}[S_T] = S_0 A_T$, the change of measure can be written

$$\frac{d\mathbb{Q}^s}{d\mathbb{Q}} = \frac{S_T}{\mathbb{E}_{\mathbb{Q}}[S_T]} = \frac{e^s}{\phi_s(-i)}$$

Hence, the density f^s under $\mathbb{Q}^s$ and the density f under $\mathbb{Q}$, both of which are densities of the log-stock price s, can be related as follows:

$$f^s(s) ds = \frac{e^s}{\phi_s(-i)} f(s) ds$$

Hence, the characteristic function $\phi_s^*(u)$ under $\mathbb{Q}^s$ can be written in terms of $\phi_s(u)$:

$$\begin{aligned}\phi_s^*(u) &= \int_{-\infty}^{\infty} e^{ius} f^s(s) ds \\ &= \frac{1}{\phi_s(-i)} \int_{-\infty}^{\infty} e^{i(u-i)s} f(s) ds \\ &= \frac{\phi_s(u-i)}{\phi_s(-i)}\end{aligned}$$

This can be substituted into the Gil-Pelaez formula to find the probability of exercise under $\mathbb{Q}^s$:

$$\begin{aligned}\mathbb{Q}^s\{s > k\} &= \frac{1}{2} + \frac{1}{\pi} \int_0^{\infty} \text{Re}\left[\frac{e^{-iuk}\phi_s^*(u)}{iu}\right] du \\ &= \frac{1}{2} + \frac{1}{\pi} \int_0^{\infty} \text{Re}\left[\frac{e^{-iuk}\phi_s(u-i)}{iu\phi_s(-i)}\right] du\end{aligned}$$

This section of the appendix can be found in Joshi (2011), and is included to ensure tractability for the reader.

Appendix B

Code (MatLab)

B.1 Heston Characteristic and Pricing Function

```
function output = HestonPrice(S0,K,sigma,r,T,lambda,rho,theta,V0)

N = 400;
u_max = 600;
k = log(K) ;
du = u_max / N ;
u = ((1:N) - 0.5)*du ;
H = alpha - 0.5 ;
nu_curl = sigma;

%"Little Trap" Characteristic Function:
a = 0.5*nu_curl^2 ;
b = @(u) lambda - rho*nu_curl*1i.*u ;
c = @(u) - 0.5*(u.^2 + 1i*u) ;
d = @(u) sqrt( b(u).^2 - 4*a.*c(u) ) ;
x_plus = @(u) (1/(2*a))*( b(u) + d(u) ) ;
x_minus = @(u) (1/(2*a))*( b(u) - d(u) ) ;
g = @(u) x_minus(u)./x_plus(u) ;
C = @(u) r*1i*T*u + theta*lambda*( T*x_minus(u) - (1/a)*log( ...
    (1-g(u).*exp(-T*d(u))).(1-g(u)) ) ) ;
D = @(u) (1-exp(-T*d(u))).(1-g(u).*exp(-T*d(u))).*x_minus(u) ;
fPhi = @(u) exp( C(u) + D(u)*V0 + 1i*u*log(S0) ) ;

%Gil-Pelaez
Int1 = real( exp(-1i*u.*k).*fPhi(u - 1i)./ (1i*u.*fPhi(-1i)) ) ;
Int2 = real( exp(-1i*u.*k).*fPhi(u) ./ (1i*u) ) ;

%Removing NaN and Inf Values:
Int1 = Int1(¬isnan(Int1));
Int1 = Int1(¬isinf(Int1));
Int2 = Int2(¬isnan(Int2));
Int2 = Int2(¬isinf(Int2));
P1 = 0.5 + (1/pi)*sum(Int1).*du ;
P2 = 0.5 + (1/pi)*sum(Int2).*du ;

output = max(S0*P1 - K*exp(-r*T)*P2,0) ;

end
```

B.2 Rough Heston Characteristic Function

```
function output = rHestonCF(a,t,dt,r,lambda,rho,nu,theta,alpha,V0,S0)

%a must be a column vector

%Creating the t vector:
t_vec = 0:dt:t ;
len_a = length(a) ;

%Riccati Equations:

%F for Rough Heston:
% F = @(a,x) 0.5*(-a.^2 - 1i.*a) + lambda*(1i.*a*rho*nu - 1).*x + ...
    0.5*(lambda*nu).^2.*x.^2 ;

%F for PM Heston Paper (ZERO MEAN REVERSION):
F = @(a,x) -0.5*a.*(a+1i) + 1i.*rho*nu.*a.*x + 0.5.*nu.^2.*x.^2;
a0k = @(k) (dt)^alpha/(gamma(alpha+2)) .* ( k.^(alpha+1) - ...
    (k-alpha).*(k+1).^alpha ) ;
ajk = @(m,k) (dt)^alpha/(gamma(alpha+2)) .* ( (k-m+2).^(alpha+1) + ...
    (k-m).^(alpha+1) - 2*(k-m+1).^(alpha+1) ) ;
akk = @(k) (dt)^alpha/(gamma(alpha+2)) ;
bjk = @(m,k) (dt)^alpha/(gamma(alpha+1)) .* ( (k-m+1).^alpha - ...
    (k-m).^alpha ) ;

%Getting the h values:
[h, Ftemp] = deal(zeros(len_a,length(t_vec))) ;
Ftemp(:,1) = F(a,0);

for kdx = 0:length(t_vec)-2
    hp = sum(bjk(0:kdx,kdx).*Ftemp(:,1:kdx+1) ,2) ;
    h(:,kdx+2) = a0k(kdx).*Ftemp(:,1) + ...
        sum(ajk(1:kdx,kdx).*Ftemp(:,2:kdx+1) ,2) + ...
        akk(kdx).*F(a,hp)  ;
    Ftemp(:,kdx+2) = F(a,h(:,kdx+2)) ;
end

%Summation for Integrals:
Int1 = sum(h(:,1:end),2)*dt ;
Int2 = dt*sum(F(a,h(:,1:end)),2) ;
output = exp( r*1i*t*a + theta*lambda*Int1 + V0*Int2 + ...
    1i*a*log(S0)) ;

end
```

B.3 Numerical Methods Implementation

```
%Initialising Parameters:
lambda = 2;
nu = 0.2;
rho = -0.6;
alpha = 0.55;
sigma = lambda*nu;
t = 1;
dt = 0.01;
tvals = 0:dt:t-dt;
tvec = 0:dt:t;
a = 1;

%Adams Scheme:
F = @(a,x) 0.5*(-1.^2 - 1i.*1) + lambda*(1i.*1*rho*nu - 1).*x + ...
    0.5*(lambda*nu).^2.*x.^2 ;
a0k = @(k) (dt)^alpha/(gamma(alpha+2)) .* ( k.^(alpha+1) - ...
    (k-alpha).*(k+1).^alpha ) ;
ajk = @(m,k) (dt)^alpha/(gamma(alpha+2)) .* ( (k-m+2).^(alpha+1) + ...
    (k-m).^(alpha+1) - 2*(k-m+1).^(alpha+1) ) ;
akk = @(k) (dt)^alpha/(gamma(alpha+2)) ;
bjk = @(m,k) (dt)^alpha/(gamma(alpha+1)) .* ( (k-m+1).^alpha - ...
    (k-m).^alpha ) ;

%Getting the h values:
[h,hpred,Ftemp] = deal(zeros(1,length(tvec))) ;
Ftemp(:,1) = F(a,0);

for kdx = 0:length(tvec)-2
    %Only Predictor
    hpred(:,kdx+2) = sum(bjk(0:kdx,kdx).*Ftemp(:,1:kdx+1) ,2) ;
    %Complete Fractional Adams
    hp = sum(bjk(0:kdx,kdx).*Ftemp(:,1:kdx+1) ,2) ;
    h(:,kdx+2) = a0k(kdx).*Ftemp(:,1) + ...
        sum(ajk(1:kdx,kdx).*Ftemp(:,2:kdx+1) ,2) + ...
        akk(kdx).*F(a,hp)  ;
    Ftemp(:,kdx+2) = F(a,h(:,kdx+2)) ;
end

%Quadrature Method:
yvals = zeros(1,length(tvec));
for idx = 1:length(tvec)-1
    yvals(idx+1) = dt./gamma(alpha).*sum((tvec(idx+1) -tvec(1:idx))
         .^(alpha-1).*F(tvec(1:idx),yvals(1:idx)));
end

figure()
hold on
plot(tvec,real(h))
plot(tvec,real(yvals), 'rx')
hold off
legend('Solution', 'Approx')

```

```
figure()
hold on
plot(tvec,real(h))
plot(tvec,real(hpred),'r.')
hold off
legend('Solution', 'Approx')
```

B.4 Rough Heston Pricing Function

```
function output = rHestonPrice(S0,K,nu,r,T,lambda,rho,theta,V0,alpha)

%Initialise Parameters
N = 400;
denom = (floor(T) + ceil((T-floor(T))/0.5) * 0.5)/0.5 ; %To ensure ...
    the dt scales with T "nicely"
dt = T/(denom*100);
u_max = 600; %Big to ensure small T values converge
k = log(K) ;
du = u_max / N ;
u = ((1:N) - 0.5)'*du ;

%Calculating Integrands
Int1 = real(exp(-1i*u*k).*rHestonCF(u - ...
    1i,T,dt,r,lambda,rho,nu,theta,alpha,V0,S0)./ ...
   (1i*u.*rHestonCF(-1i,T,dt,r,lambda,rho,nu,theta,alpha,V0,S0))) ;
Int2 = real(exp(-1i*u*k).*rHestonCF(u,T,dt,r,lambda,rho,nu,theta,...
alpha,V0,S0) ./ (1i*u)) ;

%Removing NaN and Infinity Values:
Int1 = Int1(¬isnan(Int1));
Int1 = Int1(¬isinf(Int1));
Int2 = Int2(¬isnan(Int2));
Int2 = Int2(¬isinf(Int2));

%Gil-Peleaz
P1 = 0.5 + (1/pi)*sum(Int1).*du ;
P2 = 0.5 + (1/pi)*sum(Int2).*du ;

%Answer
output = max(S0*P1 - K*exp(-r*T)*P2,0) ;

end
```

B.5 Poor Man's Heston Pricing Function

```
function output=HestonPrice(S0,K,sigma,r,T,lambda,rho,theta,V0,alpha)

N = 400;
u_max = 600;
k = log(K) ;
du = u_max / N ;
u = ((1:N) - 0.5)*du ;
H = alpha - 0.5 ;
nu_curl = sqrt(3/(2*H+2))*sigma./(gamma(H+3/2).*T.^(0.5-H)) ;

%Poor Man's Characteristic Function:
a = 0.5*nu_curl.^2 ;
b = @(u) lambda - rho*nu_curl*1i.*u ;
c = @(u) - 0.5*(u.^2 + 1i*u) ;
d = @(u) sqrt( b(u).^2 - 4*a.*c(u) ) ;
x_plus = @(u) (1/(2*a))*( b(u) + d(u) ) ;
x_minus = @(u) (1/(2*a))*( b(u) - d(u) ) ;
g = @(u) x_minus(u)./x_plus(u) ;
C = @(u) r*1i*T*u + theta*lambda*( T*x_minus(u) - (1/a)*log( ...
    (1-g(u).*exp(-T*d(u))).(1-g(u)) ) ) ;
D = @(u) (1-exp(-T*d(u))).(1-g(u).*exp(-T*d(u))).*x_minus(u) ;
fPhi = @(u) exp( C(u) + D(u)*V0 + 1i*u*log(S0) ) ;

%Gil-Pelaez
Int1 = real( exp(-1i*u.*k).*fPhi(u - 1i)./ (1i*u.*fPhi(-1i)) ) ;
Int2 = real( exp(-1i*u.*k).*fPhi(u) ./ (1i*u) ) ;

%Removing NaN and Inf Values:
Int1 = Int1(¬isnan(Int1));
Int1 = Int1(¬isinf(Int1));
Int2 = Int2(¬isnan(Int2));
Int2 = Int2(¬isinf(Int2));

P1 = 0.5 + (1/pi)*sum(Int1).*du ;
P2 = 0.5 + (1/pi)*sum(Int2).*du ;
output = max(S0*P1 - K*exp(-r*T)*P2,0) ;

end
```

B.6 Implied Volatility Surfaces and ATM Skews

```
%Table Parameters:
%alpha = 1; lambda = 0.1; rho = -0.671; V0 = 0.0392;
%sigma = 0.4061; nu = sigma./lambda; theta = 0.3156;
%r = 0.03; S0 = 100; T = 1; K = 100;

%Parameters
alpha = 0.5 + 0.0474;
lambda = 0;
rho = -0.671;
V0 = 0.06;
sigma = 0.4061;
nu = 0.4061;
theta = 0.3156;
r = 0.03 ;
S0 = 100;
dt = 0.1 ;
T = 0.05:dt:2 ;
K = 70:1:130 ;

%Setting Up Mesh for Implied Vol Surface
lenT = length(T); lenK = length(K);
[T,K] = meshgrid(T,K) ;
k = log(K./S0) ; %The log moneyness
ImpVol = zeros(lenK,lenT) ;
rImpVol = zeros(lenK,lenT) ;

%Values for IV Surface
for jdx = 1:lenK
    for idx = 1:lenT
        %Finding the Prices:
        Price = HestonPrice(S0,K(jdx,idx),sigma,r,T(jdx,idx),
             lambda,rho,theta,V0,alpha);
        rPrice = rHestonPrice(S0,K(jdx,idx),nu,r,T(jdx,idx),
             lambda,rho,theta,V0,alpha);
        %Finding Implied Vols:
        ImpVol(jdx,idx) = blsimpv(S0,K(jdx,idx),r,T(jdx,idx),Price);
        rImpVol(jdx,idx) = blsimpv(S0,K(jdx,idx),r,T(jdx,idx),rPrice);
    end
end

%Values for ATM Skew
tempIV = zeros(2,lenT) ;
rtempIV = zeros(2,lenT) ;
pmtempIV = zeros(2,lenT) ;
rPrice = zeros(2,lenT) ;
K_test = [100,100.01] ;
for jdx = 1:2
    for idx = 1:lenT
        %Finding the Prices:
        Price = HestonPrice(S0,K_test(jdx),sigma,r,T(jdx,idx),
             lambda,rho,theta,V0,alpha);
        rPrice(jdx,idx) = rHestonPrice(S0,K_test(jdx),nu,r,T(jdx,idx),
```

```
53              lambda,rho,theta,V0,alpha);
54          %Finding Implied Vols:
55          tempIV(jdx,idx) = blsimpv(S0,K_test(jdx),r,T(jdx,idx),Price);
56          rtempIV(jdx,idx) = blsimpv(S0,K_test(jdx),r,T(jdx,idx),...
57                rPrice(jdx,idx))
58      end
59  end
60  den_val = log(S0./K_test);
61  ATM = abs((tempIV(2,:) - tempIV(1,:))./den_val(2)) ; %Den_val is ...
        the log moneyness
62  rATM = abs((rtempIV(2,:) - rtempIV(1,:))./den_val(2)) ;
63
64  %Plotting ATM Skew
65  figure()
66  hold on
67  plot(T(1,:),rATM, 'bo')
68  plot(T(1,:),ATM, 'rx')
69  xlabel('\tau')
70  ylabel('ATM Skew')
71  legend('Rough', 'Classical')
72  hold off
73
74  %Rough Heston Vol Surface
75  figure()
76  subplot(1,2,1)
77  hold on
78  surf(T(1:56,:),k(1:56,:),rImpVol(1:56,:))
79  set(gca, 'YDir','reverse')
80  title('Rough')
81  xlabel('T')
82  ylabel('k')
83  hold off
84
85  %Poor Man's Vol Surface
86  figure()
87  subplot(1,2,2)
88  hold on
89  surf(T(1:56,:),k(1:56,:),ImpVol(1:56,:))
90  set(gca, 'YDir','reverse')
91  title('Poor Mans')
92  xlabel('T')
93  ylabel('k')
94  hold off
95
96  %Plotting Vol Smiles:
97  figure()
98  subplot(2,2,1) %T = 0.05
99  hold on
100 plot(k(1:56,1), rImpVol(1:56,1))
101 plot(k(1:56,1), ImpVol(1:56,1), 'r--')
102 legend('Rough', 'Poor Mans')
103 title('T = 0.05')
104 xlabel('k')
105 ylabel('IV')
106 hold off
107 subplot(2,2,2) %T = 0.25
```

```
hold on
plot(k(1:56,3), rImpVol(1:56,3))
plot(k(1:56,3), ImpVol(1:56,3), 'r--')
legend('Rough', 'Poor Mans')
title('T = 0.25')
xlabel('k')
ylabel('IV')
hold off
subplot(2,2,3) %T = 0.75
hold on
plot(k(1:56,8), rImpVol(1:56,8))
plot(k(1:56,8), ImpVol(1:56,8), 'r--')
legend('Rough', 'Poor Mans')
title('T = 0.75')
xlabel('k')
ylabel('IV')
hold off
subplot(2,2,4) %T = 1.25
hold on
plot(k(1:56,13), rImpVol(1:56,13))
plot(k(1:56,13), ImpVol(1:56,13), 'r--')
legend('Rough', 'Poor Mans')
title('T = 1.25')
xlabel('k')
ylabel('IV')
hold off
```